Lawrence Berkeley Laboratory
UNIVERSITY OF CALIFORNIA

Materials & Molecular Research Division

CALCIUM SULFATE-INDUCED ACCELERATED CORROSION

Hilary Chikezie Akuezue
(M. S. thesis)

December 1979

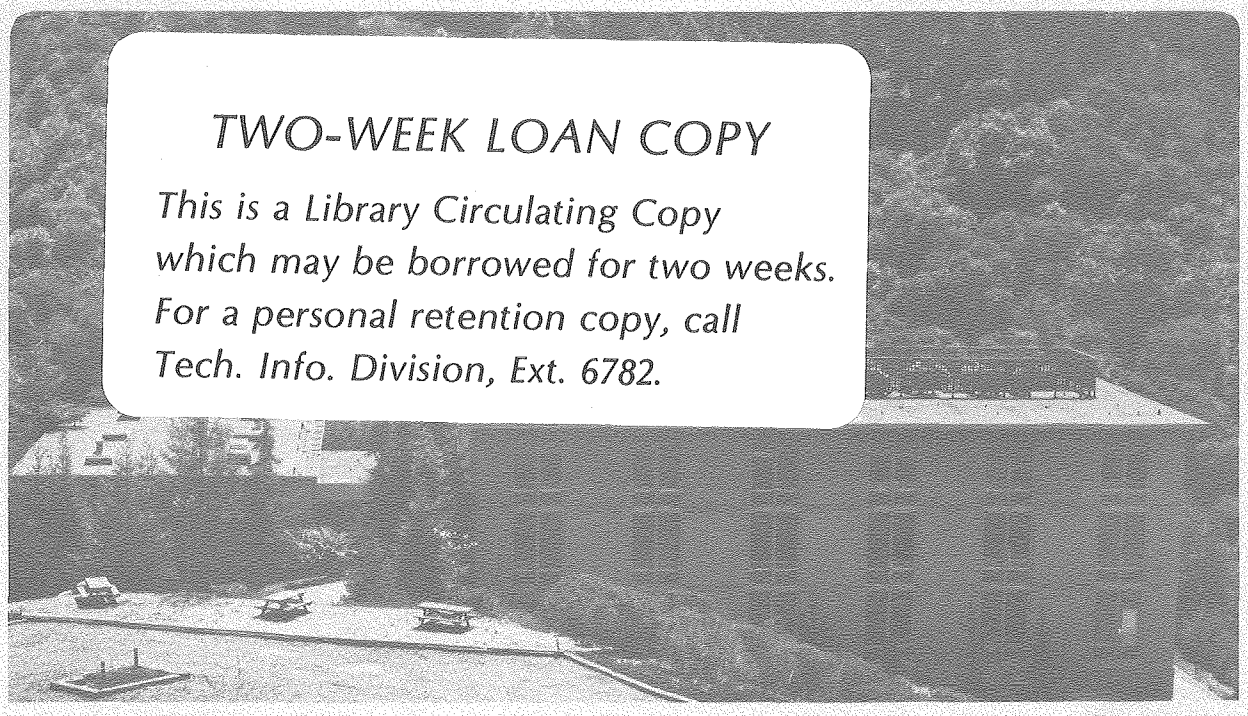

Prepared for the U.S. Department of Energy under Contract W-7405-ENG-48

DISCLAIMER

ABSTRACT

Calcium Sulfate-induced Accelerated Corrosion

By

Hilary Chikezie Akuezue

In fluidised-bed coal combustion, dolomite or limestone is fed along with the coal to absorb the sulfur. Originally, it was incorrectly expected that the spent acceptor, $CaSO_4$, would not give rise to corrosion problems. However, pilot experience has shown cases of extensive oxidation and sulfidation, which is presumably related to the calcium sulfate deposit.

The attack of $CaO/CaSO_4$ and CaO/CaS salt mixtures (1:1) on typical fluidised-bed coal combustor materials in the temperature range 850°C - 1100°C and oxygen partial pressures in the range of 10^{-19} - 1 atm. (air) were investigated using the following test materials: pure iron, nickel and chromium, Fe-20Cr, stainless steel 310 and incoloy 800. Also the effects of the introduction of sulfur-containing gases, carbon as substitute for particles of unreacted coal, and NH_3 into the $CaO/CaSO_4$ mixture were investigated.

There appear to be two aspects of $CaSO_4$-induced attack: (a) direct attack by $CaSO_4$ at low temperatures, 950°C and below, which does not involve sulfidation. In iron-base materials, the main scale contains non-protective, porous $CaFe_2O_4$ spinel and the outermost scale is a thin, sometimes loosely adhering complex calcium-iron sulfate, (b) complex calcium-iron sulfate liquid-phase attack. This occurs at high temperature, above 950°C and induces oxidation/sulfidation type of attack which is catastrophic.

A high partial pressure of sulfur appears to significantly depress

the melting point of the complex-calcium iron sulfate. Also, it depresses the melting point of $CaSO_4$. It is probable that CaS_2O_7 may form. Additions of carbon or NH_3 induce the $CaSO_4$ to decompose and hence act as a source of sulfur. High temperature also causes $CaSO_4$ to decompose. Increase in the oxygen partial pressure increases the severity of $CaSO_4$-induced attack, whilst increase in the sulfur partial pressure increases both oxidation and sulfidation.

Based on the above experimental results, a model of the $CaSO_4$-induced accelerated attack on pure iron and iron-base materials is proposed.

ACKNOWLEDGEMENTS

I would like to thank Professor David P. Whittle for his guidance during this project, and especially for his critical comments and helpful discussions at various stages of this work. Discussions with Dr. John Stringer, Electric Power Research Institute, Palo Alto, California proved especially helpful. Also, I must express my thanks to Professor Jack Washburn for his encouragement.

This work was supported by the Division of Materials Sciences, Office of Basic Research, U.S. Department of Energy, Contract No. W-7405-ENG-48.

TABLE OF CONTENTS

CHAPTER 1: INTRODUCTION

Combustion of coal in a fluidised-bed is a relatively new method of burning coal in a confined environment. The confined environment enables the waste toxic gases released during the burning of the coal to be adequately disposed of, and not allowed to escape and pollute the environment. A means for capturing most of the fuel's sulfur content during actual combustion, thus reducing the release of sulfur compounds to the atmosphere is by adding an acceptor, e.g., calcium oxide, CaO, and magnesium oxide, MgO, in the form of calcined limestone or dolomite into the bed.

In a typical coal-fired fluidised-bed combustor (figure 1), crushed coal and suitably sized acceptors are introduced into the combustor. A stream of hot air enters the base through bubble cap distributors at a superficial velocity of the order of 0.4 - 3.5 ms^{-1}. At this critical velocity, the bed material is held in suspension to give a state of boiling - fluidisation. The coal combusts at a relatively low temperature, in the range of 750 - 950^{o}C, which enables good sulfur retention by the acceptors in the bed; it is suggested that this temperature is below the ash fusion point and hence the release of alkali sulfates from the ash is less likely in the fluidised-bed combustion[1]. The limestone reacts with the sulfur dioxide, SO_2, released during the coal combustion to form calcium sulfate.

There are various ways the heat released during the combustion of the coal can be removed: by operating at high excess air and removing the heat in the exhaust gases; by passing horizontal pipes carrying water across the bed and generating steam; by heating the driving fluid for a closed-cylce gas turbine in in-bed tubes, or the bed may be used, in effect,

as the combustion chamber of a gas turbine, when operation is usually carried out at pressure.

Whereas the development of various prototype coal-fired fluidised combustion systems has been encouraged by the concern for quality of the environment, efficiency and the emergent competitiveness of coal as an alternative source of energy in the wake of the uncertainties surrounding oil, a growing concern has centered on the corrosion problems encountered by the bed materials. In addition, whereas the different forms of corrosion attack in the fluidised bed combustor have been identified, their mechanisms and source(s) are not fully understood, or as yet clearly identified. For instance, hard, adherent deposits have been identified on the in-bed components while burning coal with and without limestone additions. The growth and survival of these deposits contradict early suggestions that the erosive action of bed particles was likely to keep tubes deposit-free and might even lead to an erosion problem[1].

Tests[2] have shown that in-bed materials suffer accelerated corrosion and severe sulfidation/oxidation attacks under some circumstances, inspite of the fact that most of the aggressive sulfur compounds that could have accounted for the sulfidation have reacted with the acceptor, CaO, to form $CaSO_4$, suggests an alternative source of hot-corrosion type of attack should be present within the bed-deposit, maybe as a micro-component. Typical fluidised-bed combustor materials are shown in Table (1). It was incorrectly expected that accelerated corrosion type of attack would be unlikely in a fluidised-bed combustor because at the low temperature of combustion, the release of alkalis from the mineral constituents in the coal is relatively low. Accelerated corrosion was originally observed in the fireside corrosion of superheater tubes in conventional boilers. The mechanism[2] of corrosion appears

to involve the formation of alkali iron trisulfates, of the general form $(Na,K)_3Fe(SO_4)_3$.

Nevertheless, recent emphasis towards isolating the cause and source of the severe corrosion attack on the in-bed components of a fluidised-bed combustor is centered on the deposits. The fundamental importance of such deposits is now clearly evident as numerous evidence is relating the cause of the severe corrosion to possibly micro-components contained in the deposit. Chemical analysis of the deposits has been carried out by CRE[2], and these were found to contain particles of calcium sulfate, $CaSO_4$, and calcium oxide, CaO.

According to the CRE test[3], a typical deposit in the fluidised-bed contains about 50 per cent $CaSO_4$ and 40 per cent CaO, therefore, the role of the spent acceptor, $CaSO_4$, on the corrosion behavior of the fluidised-bed combustor materials should be considered. In assessing the role of spent acceptor as a potential cause of severe corrosion attack in fluidised-bed combustors, the role of calcium sulfide, CaS, as one of the stable products during the reaction of the acceptor, CaO, with sulfur or sulfur dioxide inside the bed has to be considered and examined in isolation or with $CaSO_4$, the chief by-product.

Furthermore, whilst the state of fluidisation encountered within the fluidised bed combustor serves to ensure thorough mixing of the bed content as well as a uniform gas environment, pilot tests[4], indicate there are micro-environments inside the bed which fluctuate from oxidising to reducing conditions. The micro-environment is established due to the side-by-side existence of air bubbles and combusting coal particles. Each coal particle is, in principle, surrounded by an envelope in which the oxygen activity falls from its value in the sorrounding gas to a value equal to the C/CO equilibrium at the surface temperature,

but it is probable that this envelope is quite small in extent, because of the rapid heat exchange in the bed. At anytime, the bed will contain perhaps one per cent coal, so on average each coal particle is 4 - 5 diameters from the next. The gas outside these small combustion envelopes will exchange with the air in the bubbles, and will thus have an oxygen activity below that of the overall system (0.03 atm. typically); but in the absence of more information, the actual activity is difficult to estimate.

Also, the heat transfer tubes traversing the bed are swept by various sizes of rising bubbles which have the ability to either split or coalesce. Each of these bubbles carries a wake of particles, thus causing an upward drift of particles. Overall, it has been noted that there is a marked tendency for the degreee of vertical mixing to exceed lateral mixing and this can also help to establish regions of micro-environments which may fluctuate from oxidising to reducing conditions.

A. Corrosion

Degradation of materials when due to the chemical reaction occurring between one or more elements of the material and oxygen is called oxidation. However, when the reaction involves sulfur, the degradation is known as sulfidation. The oxygen and sulfur can be in gaseous or liquid phase. Thus, a corrosion reaction involves the degradation of the material due to either oxidation or sulfidation, or both.

The product of corrosion reaction is called the scale, so that the scale can be either a sulfide, or an oxide, or a combination of both. Once a scale is formed during a corrosion reaction, the scale acts as a barrier against further direct contact between the reactants. In this way, subsequent degradation will depend on the transport rate of the reactants, or one of the reactants across the scale. Thus, if

an alloy is to resist oxidation, for instance, it must form a protective oxide scale on its surface; the scale then acts as a barrier which minimizes further interaction with the environment. An oxide is said to provide a good barrier to protection when the transport of reacting ions through the oxide is slow. Most oxides are non-stoichiometric and contain defects: cation and anion sub-lattices permitting lattice transport, or more extended defects, such as sub-grain and grain-boundaries acting as short circuit diffusion paths. In addition, if the protective scale is to function as an effective barrier, it must remain adhered to the alloy and the detailed morphology of the alloy/scale is critical. Extensive work has been done by Whittle[5][6] et al on the critical parameters affecting oxide adherence.

Chromium and aluminum oxides both have slow growth rates, i.e., transport of reacting ions through their oxides are slow. Furthermore, they deviate very minimally from their stoichiometric compositions. Al_2O_3, although possessing all of the above good protection properties, does not possess a good adhering property. Consequently, Al_2O_3 scales frequently spall off. This results in the depletion of the Al content of the alloy below the minimum necessary to maintain or form a continuous protective Al_2O_3 layer. In the last five years, successful techniques have been developed to improve the adherence of Al_2O_3 oxides to their substrates[4].

Simultaneous oxidation and sulfidation can take place. The most common environment in which this is encountered is in the burning of fossil fuels. Virtually all fossil fuels contain sulfur as an impurity and when they are burned, whether in a turbine, in fluidised beds, or in conversion processes, such as coal gasification or liquefaction, they generate atmospheres that contain sulfur compounds. In turn, the sulfur

compounds can lead to sulfidation problems; and formation of metal sulfides always accelerates the rate of material degradation. Sulfur competes with oxygen for the principal scale forming elements, Cr and Al, thereby interfering with the process of protective scale formation; and because sulfides are far more defective than corresponding oxides, they thicken more rapidly.

Figure (2a) is a schematic metal-sulfide-oxide stability diagram. The regions - as a function of oxygen and sulfur potential - where metal sulfide or oxide are stable are outlined. First, consider gaseous atmospheres corresponding to the shaded area (as in 'A'); such atmospheres are typical of coal conversion, in which the oxygen activity is high enough to form the oxide, and the sulfur potential is high enough to form the sulfide.

In general, the atmosphere will have oxygen and sulfur potentials that will support either, but not both, oxide or sulfide formation (to the right or left of the oxide/sulfide co-existence line, respectively). Joint formation of oxide and sulfur in equilibrium with the atmosphere demands a unique gas composition (corresponding to the co-existence line).

There are other conditions, however, under which sulfide and oxide can form together at the scale/gas interface. For example, localized changes in gas composition, due to restricted access, can occur and act to shift the composition to point 'B'. Such conditions can exist under ash deposits in coal-fired utilities; rate-limiting diffusion in the gas phase is also a possibility.

The formation of sulfides within or below the oxide scale is more common. The obvious conclusion is that sulfur can penetrate growing oxide layers, and that it might be over optimistic to depend simply on oxide layers for protection from sulfidation under conditions in which

a conjoint attack is possible. Two possibilities present themselves: dissolution followed by lattice diffusion; and transport of gaseous molecules via physical defects, such as pores and micro-cracks. These are alternative and parallel mechanisms and may operate together. A gas composition such as that at point 'C' in figure (2a), (now in the hatched area) is typical of a process atmosphere from a low-sulfur fuel. Sulfide formation cannot be produced in such an atmosphere if sulfur dissolves in the oxide and transports to the metal/scale interface. There is no mechanism by which the sulfur activity can be increased (path (i) in figure (2a)).

If, for example, SO_2 molecules can penetrate the scale through micro-crack or physical defects, however, then changes in gas composition within the restricted volume of the crack or pore can occur. Effectively, removal of oxygen to form oxides increases the sulfur potential to the point at which sulfide may be formed (path (ii)). The effective gas composition within the porous scale moves from the cross-hatched area into the shaded area (figure (2a)). Here differences are expected between the combusted and process atmospheres. In the combusted atmosphere, sulfur is present mainly as SO_2. Consequently, the sulfur potential is closely linked to the oxygen potential through the SO_2 decomposition equilibrium. In process atmospheres, in which there are significant concentrations of hydrogen, the sulfur is present as H_2S and its potential is virtually independent of the oxygen potential.

The fluidised-bed coal combustion corresponds to a combustion process in which the sulfur mainly is SO_2 and the sulfur potential is therefore closely linked to the oxygen potential through SO_2 decomposition. However, due to locally poor mixing of the charge inside the fluidised-bed and occurence of $CaSO_4$-containing deposits on the in-bed components,

regions typical of process or reducing atmospheres can be present within the fluidised-bed coal combustor operating with dolomite and limestone additions. A reducing atmosphere, for instance, can reduce the $CaSO_4$ or cause it to decompose, releasing sulfur. If the reducing atmosphere contains hydrogen species in addition, the sulfur is present as H_2S and its potential is virtually independent of the oxygen potential. A sulfatic deposit like $CaSO_4$ may be reactive under reducing conditions in addition to decomposing. However, the decomposition of the $CaSO_4$ is such that the function of the salt deposit is to fix the reaction potential of sulfur and oxygen in much the same way that the interrelated gas equilibria do. Besides, there are additional possibilities of direct reaction between the salt and the protective oxide.

Thus, the degradation of a material due to corrosion is further influenced by the degradation of the protective oxides: (a) by sulfur-bearing gases; (b) by reactive deposit, e.g, $CaSO_4$; (C) by H_2, C etc. bearing gases.

Furthermore, in the fluidised bed coal combustor operating with limestone addition, the deposit on the in-bed components consists mainly of $CaSO_4$ and CaO. The deposit can be porous, semi-porous, or compact. If the deposit is compact and homogeneous, it can act as an oxygen barrier. Therefore, towards the metal/deposit interface the oxygen potential is low, and the $CaSO_4$ can decompose. In semi-porous deposits, pockets of isolated SO_2 gas depleted in oxygen due to local oxidation can fix relatively high sulfur potential, enough to sulfidise the oxides. Porous deposits act as stagnant local regions in which the oxygen content is rapidly decreasing as the oxidation continues, thereby promoting high sulfur potentials with time.

All of the above operating modes can occur simultaneously or in combination in which case, one mode may be characteristically dominant.

B. Previous Corrosion Studies In Fluidised Bed Combustors

There have been few systematic studies of corrosive attack in fluidised-bed coal combustion systems, and most relate to work carried out by the Coal Research Establishment (CRE) of Great Britain and sponsored by the Electric Power Research Institute (EPRI) of U.S.A.

The EPRI project was mainly a pilot test to assess the overall corrosion performance or resistance of various sections of the fluidised-bed combustor system while burning different grades of coal with or without dolomite or limestone additions. The CRE test consists of, among others, four horizontal tubes across the bed, one cooled by passing air at room temperature and a constant temperature was maintained by controlling the flow rate on the mean of four thermocouples inserted into the wall of each tube. Each tube consisted of a number of 50 mm o.d. x 22 mm rings of different alloys clamped together. The pilot tests were run between the temperature range 540^{o}C to 900^{o}C for 2,000 hours and at the end of the first 1,000 hours, highly corroded coupons were replaced for the next 1,000 hours run.

At 900^{o}C, the CRE test reported that in some cases, the deposits apeared molten, but added that this was not borne out by later tests which gave decomposition temperatures of the deposits considerably higher than 900^{o}C. However, the CRE test failed to account for the molten deposits in the first place. At 540^{o}C and 650^{o}C, the low chromium steels suffered extensive oxidation with a corresponding decrease in the tube wall thickness. The high chromium ferritic steels showed moderate sulfidation at 540^{o}C with some increase at 650^{o}C. At 760^{o}C and 840^{o}C, incolloy 800, inconnels 601, 617, 671, hastelloy X, HA 188 and inconel 690 suffered severe sulfidation accompanied in most cases by considerable pitting and localised thick scales above the pits. Sulfidation also

occurred on type 347 and type 310, but with an absence of pitting. As the temperature increased, sulfidation became more severe. Also, more attack was observed when limestone was added to reduce the sulfur dioxide emission level. The CRE reports, to a very good extent, demonstrated that accelerated oxidation and sulfidation occurs within the bed of the fluidised-bed combustors during pilot tests, but no systematic tests were carried out to determine the various variables involved in the attack.

A more detailed study of the corrosion environment within the fluidised bed was carried out by CRE[2] using medium carbon steel, 1Cr-½Mo, 2-¼Cr-1Mo, 12Cr steel, types 316 and 347. The steels were obtained as two in o.d. cold drawn tubes, fully heat treated. These coupons were stationed at different positions inside the pilot plant. After corrosion testing, the test specimens were examined visually, photographed, then the majority were descaled for weight loss measurements. The results presented below represent a summary of the whole program.

Negligible deposition was found, with only slight accumulations on tubes near the coal nozzles and on tubes in the freeboard. These generally had the same composition as the ash, although in some isolated instances there was a slight enrichment in alkalis and sulfur. The lack of deposition was mainly attributed to reduced volatilization of alkalis because of the low combustion temperature compared to the conventional boiler, with possibly some contributions from the scouring action of the bed.

In general, specimens in the freeboard of the combustor were corroded less than in-bed specimens. Typical (descaled) weight losses after 1,000 hours are shown in Table (2) and weight loss-time curves

are shown in figures (3) and (4). In these diagrams a line has been drawn representing what CRE considers to be an acceptable rate of weight loss: 30μg/cm^{2}h, which is equivalent to a penetration rate of 1.5 x 10^{-6} in/hr assuming no preferential loss around the circumference of the tube and no intergranular penetration and, of course, a linear rate, which may not be the case.

Specimens exposed at or below their normal maxium working temperature in conventional plants did not suffer significant intergranular sulfidation. At 700^{o}C intergranular penetration of the high-chromium steels were observed after only 100 hours, with oxidation penetration of 15μm and in some places sulfidation penetration to 10 - 20μm. Coupons held in the bed at 850^{o}C showed intergranular sulfidation to depths of 30 - 50μm in the 100 hour tests, and 30 - 60μm in the 1000 hour tests. For the low-chromium steels, sulfidation was a particular problem with the 2-¼%Cr-1%Mo alloy at 600^{o}C, with maximum penetration of 70μm. Carburisation was not detected. The nature of the coal was not thought to have exerted a major effect on corrosion in the fluidised-bed combustor. Operation under sub-stoichiometric conditions caused little change in the corrosion rate of in-bed tubes, but the corrosion rate of the freeboard tubes was increased. In very strongly reducing conditions, however, when loss of fluidisation occurred, the corrosion rate of in-bed tubes was increased four-fold. Increased sulfide penetration was observed for tests with limestone or dolomite additions to the bed, particularly for the high-chromium steels at 700^{o}C and 850^{o}C, but the reasons were not clear.

Earlier crucible test[8] experiments suggested that mixtures of calcium sulfate and graphite can induce sulfidation attack in the absence of any apparent molten phase, although more extensive study still needs

to be carried out in this respect. Furthermore, recent tests funded by EPRI[9] show that localized hot regions differing by as high as 200°C from the operating temperature are possible within the bed due to the presence of the deposits. Thus, a bed operating at 850°C can expect to have local hot regions at about 1,000°C or higher. The obvious implication of the above is that $CaSO_4$ can then start decomposing locally, thereby acting as a source of sulfur.

C. Objectives

This study is aimed at investigating the factors responsible for the corrosion associated with spent acceptors, $CaSO_4$, in fluidised-bed coal combustors, and attempts to determine how these are related to the operating variables. Typical materials for fluidised-bed components include mainly stainless steel and other iron-base alloys.

In a fluidised-bed containing an acceptor, the bed material consists of a mixture of CaO, $CaSO_4$, ash and uncombusted coal. Calcium oxide, CaO, is added to absorb the SO_2 emitted during the combustion of the coal and form calcium sulfate, $CaSO_4$. Thus, $CaSO_4$ and CaO constitute the large majority of the bed and deposits on the tubes accounting for about 50 per cent and 40 per cent of the entire bed deposit respectively. The environment condition can then best be envisaged in terms of the Ca-O-S stability diagram which presents the phases present at equilibrium as a function of oxygen and sulfur potentials. This is shown in figure (2), and has been calculated according to the following reactions:

$$CaS + 2O_2 = CaSO_4 \qquad (A)$$

$$K_A = \frac{a_{CaSO_4}}{a_{CaS} \cdot P_{O_2}{}^2}$$

and assuming $a_{CaSO_4} = a_{CaS} = 1$:

$$K_A = \frac{1}{P_{O_2}^2} \qquad (A_1)$$

$$2CaS + O_2 = 2CaO + S_2 \qquad (B)$$

$$K_B = \frac{a^2_{CaO} \cdot P_{S_2}}{a^2_{CaS} \cdot P_{O_2}}$$

for pure CaO and CaS:

$$K_B = \frac{P_{S_2}}{P_{O_2}} \qquad (B_1)$$

$$2CaO + S_2 + 3O_2 = 2CaSO_4 \qquad (C)$$

$$K_C = \frac{a^2_{CaSO_4}}{a^2_{CaO} P_{S_2} \cdot P^3_{O_2}}$$

assuming pure $CaSO_4$ and CaO:

$$K_C = \frac{1}{P_{S_2} \cdot P^3_{O_2}} \qquad (C_1)$$

T^oC	750	850	950
Log K_C	50.5	43.25	38
Log K_B	10	9	8.3
Log K_A	30	26	23

Since $CaSO_4$ and CaO constitute the majority of deposit and bed, it might tentatively be assumed that they are at equilibrium according to reaction (C); therefore, equation (C_1) represents the line separating the CaO and $CaSO_4$ regions in the Ca-O-S stability diagram - figure (2). The slope of the $CaSO_4$/CaO boundary line indicates the local atmosphere depends on P_{O_2}. For instance, increasing P_{O_2} corresponds to decreasing P_{S_2}, while decreasing P_{O_2} corresponds to increasing P_{S_2}. A direct measurement of the oxygen activities inside and above the bed in the fluidised-bed combustor has been carried out by Cooke, et al[7], using a solid electrolyte probe. Within the bed, the probe indicated an oxygen activity of 10^{-12} atm. at 850°C in normal operation, with occasional excursions to higher values due to bubbles passing up through the bed past the probe. In figure (2), an oxygen activity of 10^{-12} atm. at 850°C corresponds to a sulfur activity of 10^{-7} atm. providing CaO and $CaSO_4$ are in equilibrium. Furthermore, consider the equilibrium sulfur partial pressures for the system: Cr/CrS and Fe/FeS at 850°C (1123°K) from the following equations:

$$Cr + 1/2S_2 = CrS, \quad \Delta G^\circ = -48400 + 13.4T \qquad (1)$$

$$K_{1123°k} = 3.27 \times 10^6$$

$$P_{S_2} = 10^{-13} \text{ atm.}$$

$$Fe + 1/2S_2 = FeS, \quad \Delta G^\circ = 1/2(-71820 + 25.12T) \qquad (2)$$

$$K_{1123°k} = 10^4$$

$$P_{S_2} = 10^{-8} \text{ atm.}$$

Hence, the corresponding sulfur activity as calculated from the $CaO/CaSO_4$ equilibrium at $P_{O_2} = 10^{-14}$ atm. at 850°C is higher than the equilibrium sulfur activity for the Cr/CrS and Fe/FeS systems at the same temperature and P_{O_2}. That is, sulfidation of deposit-laden in-bed metal components within

the fluidised-bed is very possible at normal operating conditions according to the Ca-O-S stability diagram. For instance, addition of graphite to the $CaSO_4/CaO$ deposit has previously been shown to induce sulfidation of iron-base alloys at 950°C in static air[8]. The graphite addition to the $CaSO_4$ was made on the assumption that the graphite will establish low oxygen activity thereby inducing the $CaSO_4$ to decompose, the decomposition of $CaSO_4$ being all that is needed to provide the sulfur necessary for the sulfidation attack. The experimental results indicate graphite can induce $CaSO_4$ to decompose at 950°C[7], but whether this was as a result of low oxygen activity established by the graphite is debatable. If graphite induces $CaSO_4$ to decompose as a result of the low oxygen activity established by the CO_2/CO equilibria, arrived at, and not involving $CaSO_4$ in the process, then low oxygen activity established via gaseous CO_2/CO mixture will also induce the $CaSO_4$ to decompose and similarly induce sulfidation of iron-base alloys.

As a consequence, the effects of these local atmosphere conditions in combination with $CaO/CaSO_4$ mixture on the fluidised-bed materials seem important. In the first instance, the oxygen pressures (10^{-19} and 10^{-11} atm.) have been fixed via CO/CO_2 gas mixture, expecting the $CaSO_4$ or CaS to decompose and fix the corresponding sulfur partial pressures. The oxygen activity in a CO/CO_2 gas mixture is related by the following equations:

$$2CO + O_2 = 2CO_2 \qquad (4)$$

$$P_{O_2} = 1/K_4 \left(\frac{P_{CO_2}}{P_{CO}} \right)^2$$

an alternative approach is to use H_2/H_2O mixtures according to the following equilibria:

$$2H_2 + O_2 = 2H_2O \qquad (5)$$

$$P_{O_2} = 1/k_5 \left[\frac{P_{H_2O}}{P_{H_2}}\right]^2$$

where K_4 and K_5 are the appropriate equilibrium constants and which are given below:

T^oC	700	750	800	850	900	950
Log K_4	21.262	19.79	18.432	17.208	16.086	15.036
Log K_5	20.922	19.618	18.436	17.354	15.748	15.436

In order to control the P_{O_2} at 10^{-15} atm., for instance, requires

$$\frac{P_{CO_2}}{P_{CO}} \text{ or } \frac{P_{H_2O}}{P_{H_2}}$$

ratios of approximately 250 and 200 respectively and these are difficult to control. However, at least two different oxygen pressures, 10^{-19} and $10^{-11.5}$ atm. were fixed via the CO/CO_2 gas mixtures. The reason for particularly choosing these two oxygen pressures is because 10^{-19} atm. is a relatively low oxygen activity and if the suggestion that low oxygen potentials induce the $CaSO_4$ to decompose is correct then expect sulfidation attack; on the other hand, $10^{-11.5}$ atm. of oxygen is about the recorded equilibrium oxygen pressure in a fluidised-bed coal combustor operating at 850^oC.

Besides, both the oxygen and sulfur activities can be fixed using $CO_2/H_2/H_2S$ or $CO/CO_2/SO_2$ gas mixtures in which case the role of the $CaSO_4$ is completely redefined in terms of whether there is any direct chemical

or solid-state interactions between the protective oxide and the $CaSO_4$ salt. The direct reaction between the $CaSO_4$ and the protective oxide has also been investigated by coating the test pieces with $CaSO_4$ paste or oxidising the samples embedded in the $CaO/CaSO_4$ mixture in static air. Effects of temperature on the $CaSO_4$-induced attack have also been studied. Since the 50 per cent $CaSO_4$-containing deposit also contains small particles of unburnt coal as micro-constituents and the gaseous environment in the fluidised-bed combustor contains NH_3 as a micro-component, the effects of these 'contaminants' on the corrosion potentials of the $CaSO_4$ have also been investigated and compared.

Thus, the investigation is aimed at demonstrating with the aid of the Ca-O-S equilibrium diagram and other operating parameters that $CaSO_4$ can cause unacceptable degradation of in-bed components of the fluidised-bed coal combustor operating with limestone or dolomite additions as sulfur sorbents. Based on the above study, a model of the mechanism(s) of the $CaSO_4$-induced accelerated attack is attempted (for iron-based materials).

CHAPTER 2: EXPERIMENTS

A. Experimental Procedures

Earlier work by Whittle et al[8] had shown that iron base materials when oxidised in graphite-containing $CaSO_4$ at 950°C in static air suffered sulfidation attack, but whether the low oxygen activity as induced by the graphite via CO/CO_2 equilibria was the cause of the $CaSO_4$ decomposition is debatable. To investigate the above, a more controlled experiment involving $CaSO_4/C$ and $CaSO_4/CO_2/CO$ respectively was designed; first the experiment at 950°C using $CaSO_4/C$ is repeated. 950°C is a relatively high temperature, because most fluidised-beds operate at 850°C and below, therefore, the comparison between the attacks by $CaSO_4/C$ and $CaSO_4/CO_2/CO$ have been carried out at 850°C.

The attacks of $CaSO_4/C$ (1:1) on typical fluidised-bed combustor materials at 950°C and 850°C in static air were investigated using the following test materials:

1. pure iron (99.94% purity)
2. pure chromium
3. pure nickel
4. Fe-20Cr (as cast)
5. incoloy 800
6. stainless steel 310

Samples of IN 800, Fe-20Cr and st. st. 310 having 12 x 8 x 2 mm average dimensions were prepared by grinding on SiC metallographic polishing papers to 600 grit. All samples used in this experiment have above dimensions except when otherwise stated. The samples were degreased and finally washed in alcohol and then dried. The $CaSO_4$ is optically pure grade (99.99%).

The test samples were embedded in $CaSO_4/C$ (1:1) mixture contained

in a recrystallized alumina boat and then introduced into a horizontal furnace at 950 and 850^{o}C respectively. While introducing and removing the boat into and from the furnace, considerable care was taken to avoid the cracking of the re-crystallized alumina boat due to thermal shock. The test samples were oxidised for different times in order to investigate the effect of time and hence the rate of attack. The test samples after each set of tests were mounted in Klarmount mounting compound and polished. The cross-sections were examined under the light microscope and the interesting features were noted. Also, all the test samples were examined quantitatively for phases present in the scale or regions of attack using the scanning electron microscope and fitted with Edax attachment. Electron image and X-ray maps of some of the cross-sections are shown in the next heading under results.

To investigate whether the low oxygen activities as established by the graphite via the CO_2/CO equilibrium is the cause of the $CaSO_4$ decomposing to release sulfur for sulfidation attack, an apparatus was set up to investigate the attacks by $CaO/CaSO_4$ and CaO/CaS salt mixtures (1:1) on IN 800, st. st. 310 and Fe-20Cr at low oxygen (10^{-19} atm.), fixed via CO_2/CO gas mixture at 850^{o}C. The Ca-O-S stability diagram, figure (2), shows that at 10^{-19} atm. oxygen pressure, and 850^{o}C, the equilibrium phases are CaS and CaO so that the $CaSO_4$ /CaO mixture is unstable. Also, since the equilibrium oxygen activity within the fluidised-bed operating with limestone addition at 850^{o}C is about 10^{-12} atm., the test samples were also tested at relatively high oxygen activity of $10^{-11.5}$ atm. Again, the oxygen activity was fixed via CO_2/CO gaseous equilibria.

The apparatus for all tests involving the fixing of one or all of the gaseous components, O_2 and S_2, consists of a vertical muffle furnace with three built-in compartments into which three quartz tubes with

two gas outlets respectively, can be lowered. Each quartz tube consists of two matching parts which can be made air-tight by means of adjustable clamps. The best overall view of the apparatus is shown in figure (6).

In each run of the experiment, about 3 mm depth of the salt mixture was first introduced into the quartz tube, then the samples were gently lowered and covered with the salt mixture. In the first trial runs, continuous flow of the CO/CO_2 gas mixture was maintained throughout the duration of each experiment and very little attack was observed. To test whether the flow of the gas was contributing to the effect of no-attack, 8 x 1 cm o.d. quartz tube filled with $CaO/CaS/CaSO_4$ and Fe-20Cr samples, was evacuated and sealed. The sealed-off quartz tube was maintained at $850^{o}C$ for 100 hours. Sulfidation attack was observed in Fe-20Cr alloy contained in the sealed quartz tube. This merely shows that Fe-20Cr when embedded in $CaSO_4$ and oxidised in a stagnant condition will in the course of the oxidation deplete the available oxygen as a result of formation of Cr_2O_3 and FeO. Further growth of Cr_2O_3 or Feo will be accomplished by removal of oxygen from $CaSO_4$ thereby causing the release of sulfur for sulfidation. In figure (5) is shown the Ca-O-S stability diagram at $850^{o}C$ on which the Fe-O-S and Cr-O-S stability diagrams are superimposed. In this figure (5), it is seen that $CaSO_4$ at low oxygen pressures will be unstable relative to FeO, FeS, Cr_2O_3 and CrS. In subsequent runs the gas was turned on only for the first 15 - 20 minutes of the experiment to allow the salt mixtures to equilibriate. The latter technique produced considerable attack in most oxygen pressures.

To further investigate the mechanism of the attack, thin coatings of $CaSO_4$ were deposited on pure iron samples (2 mg/cm^2) by spraying very dilute colloid of $CaSO_4$ onto samples placed on a hot plate. Isothermal weight measurements were carried out at the following oxygen pressures:

1. $10^{-11.5}$ atm.
2. 10^{-14} atm.
3. 10^{-19} atm.

} constant flow rate of CO/CO_2 gas mixture ~ 1,000 CC/min

the first of which was mounted for metallographic examination. Also, micro-probe analysis was carried out on the scales formed.

A paste of $CaSO_4$ was moulded onto the samples and allowed to harden under low heat and just before the paste completely hardened, excess paste was cut off with a razor blade leaving about 2 mm uniform thickness of paste around the samples. The $CaSO_4$ paste-coated samples were oxidised in static air for 100 hours and at the end of the exposure, the adhering $CaSO_4$ paste was gently separated from the scales formed on the samples and examined visually and it appears yellowish in color immediately next to the scale. The yellowish looking deposit next to the scale is confined to a relatively thin section. The pH of this thin yellowish layer was determined (average pH: 7.3). For comparison, the pH of the original $CaSO_4$ was also determined (average pH: 6.2).

To observe the $CaSO_4$/metal and subsequent $CaSO_4$/oxide interface during the $CaSO_4$ induced accelerated oxidation, a hole 0.131 in o.d. was drilled on a 1.24 x 0.1.56 in o.d. cylinderical pure iron sample and $CaSO_4$ was packed into the hole. The upper surface of the cylinder was polished and the hole very well cleaned before the $CaSO_4$ was packed into the hole. Also, care was taken to prevent contamination of the polished surface by the $CaSO_4$ during packing. This ensured the $CaSO_4$/metal interface was defined initially. The sample was then oxidised at 850°C in a hot stage microscope. The $CaSO_4$/metal interface was examined at 850°C temperature by using a stereo microscope. To record results from these experiments, motion picutres of the reaction were obtained which allowed the accelerated oxidation process to be studied.

To simulate and investigate a situation within the fluidised-bed coal combustor operating with limestone addition and in which the limestone had been discontinued after a while, IN 800, Fe-20Cr and st. st. 310 were oxidised embedded in $CaSO_4$ deposit under a $H_2S/H_2/CO_2$ gaseous mixture (3.5%H_2, 1%H_2S, bal. CO_2) which was allowed to flow through for the first fifteen minutes of a 100 hour test at 850°C. Assuming thermodynamic equilibrium is established, the gas mixture should correspond to 10^{-4} atm. of sulfur at 850°C. Schematic representation of the above situation is shown in figure (7).

Samples were also oxidised, embedded in $CaSO_4$ in static air at different temperatures to determine the effects of temperature on $CaSO_4$-induced attacks. NH_3 gas is present during the combustion of the coal in the fluidised-bed combustor and therefore the effect of this gaseous trace on $CaSO_4$-induced attack was also investigated and compared with that of graphite.

The results are presented under the next heading.

B. Results Of Corrosion Experiments

In the Objectives (see pp. 12-17) it was mentioned that Whittle et al[8] had shown that IN 800 when oxidised in graphite-containing $CaSO_4$ salt at 950°C in static air suffers sulfidation attack. It is postulated that the graphite induces a low oxygen potential around the $CaSO_4$ thereby causing it to decompose and act as a source of sulfur. So far no controlled experiment has been carried out to investigate the accuracy of this postulate. Furthermore, 950°C is relatively high when compared to 850°C, the normal working temperature of most fluidised-bed coal combustors.

In figure (8) is shown the optical photograph of the cross-section of the scale formed on IN 800 after oxidation in $CaSO_4$/C (1:1) at 950°C

for twelve hours in static air. The dark areas in the micrograph are regions where the incoloy has suffered an attack. The white regions are the unattacked alloy matrix. The boundary between the attacked and unattacked alloy matrix is not defined. In some places, the unattacked alloy matrix is completely surrounded by the attacked regions. Therefore, the attacked regions do not provide a protective barrier against further attack. Deeper in the alloy matrix, the attack tends to occur along the grain-boundaries. The maximum depth of internal attack is about 0.03 mm. In figure (9) are shown the results of the scanning electron analysis of the cross-section of the scale formed on IN 800. The Edax analysis of a point within the grain-boundaries attack shows a high peak intensity of sulfur and chromium, indicating that the grain-boundary phase is primarily chromium sulfide. The titanium, iron and aluminum peaks are relatively small and it is unlikely any of their sulfides is in much quantity. Also, the Edax analysis of a point near the top of the scale shows a high chromium peak, but in addition, an iron peak which is higher than that associated with the grain-boundary attack can be seen. Furthermore, a calcium peak is present. The X-ray maps show the distributions of the different elements. In the chromium map, the regions surrounding the grain-boundaries where chromium sulfides have formed are correspondingly depleted in chromium. Therefore, the migration of chromium towards the grain-boundaries to form CrS results in the depletion of chromium in the vicinity of the grain-boundary. Consequently, more noble components of the alloy, e.g., iron, nickel and titanium, become oxidised as the chromium is tied. The CrS later gets oxidised and the sulfur diffuses deeper into the alloy matrix. The process is self-sustaining once it starts and propagates at a rate that depends on the oxidation rate of CrS which is considerably faster

than the rate of oxidation of chromium. The overall result is that the main scale consists of a mixture of oxides as the X-ray maps show; iron and nickel are contained in the outermost scale.

In figures (10) are shown the optical micrographs of the cross-sections of the scale formed on Fe-20%Cr and stainless steel 310 after oxidation in $CaSO_4$/C mixture at 950^{o}C for twelve hours in static air. The attack on Fe-20Cr is severe and the main outermost scale is detached. It is not certain whether the detachment occurred during oxidation or during cooling due to thermal stress. However, the region of internal attack can be seen below the main adhering scale, penetrating to a depth of about 3×10^{-2} mm into the matrix. The internal attack is also chromium sulfide and the mechanism of attack and propagation is similar to that of figure (8), i.e., sulfur diffuses into the alloy along the grain-boundaries. Chromium migrates towards the grain boundary and forms CrS. The adjoining regions around the grain-boundary becomes depleted in chromium so that the more noble iron gets oxidised. The chromium sulfide gets oxidised releasing the sulfur which diffuses further into the alloy. In this way, the main scale consists of a mixture of iron and chromium oxides. Calcium is also present in the outermost scale. The cross-section of stainless steel 310 (figre 9B) shows mainly internal attacks of CrS and Cr_2O_3. The depth of maximum penetration of CrS is about 3×10^{-2} mm. Stainless steel 310 is the least attacked of the three alloys oxidised in $CaSO_4$/C mixture at 950^{o}C in static air for twelve hours.

In figures (11) are shown the optical micrographs of the cross-sections of the scales formed on the three alloys (IN 800, Fe-20Cr and st. st. 310) after oxidation in $CaSO_4$/C mixture at 950^{o}C for fifty hours in static air. At longer times, the effect of carbon in inducing $CaSO_4$

to decompose diminishes as the graphite and $CaSO_4$ are consumed and as the sulfur is oxidised away.

In figure (12) are shown the scanning electron image and X-ray maps of a region on the cross-section of the scale formed on Fe-20Cr after oxidation in $CaSO_4$/C in static air at 850°C for 100 hours. The sulfide region in figure (12) is very confined and incidentally, this is the only region with sulfide penetration in the entire cross-section. Generally, sulfidation attack by graphite-containing $CaSO_4$ diminishes with temperature. Also, IN 800 and stainless steel 310, when oxidised in $CaSO_4$/C at 850°C for 100 hours, suffered insignificant sulfidation confined to very small sulfide precipitates below the scale. The sulfide phases in most cases are so small that they can only be seen at magnification greater than 10,000

C. Effect of Controlled P_{O_2} On $CaSO_4$-Induced Corrosion

It is suggested that the graphite established low oxygen activity around the $CaSO_4$, thereby causing it to decompose at 950°C. At 950°C, there are two possible reactions between graphite (C) and oxygen in static air:

$$C + O_2 = CO_2 \quad (A)$$

$$C + \tfrac{1}{2}O_2 = CO \quad (B)$$

Therefore, expect the calcium sulfate to similarly decompose when a low oxygen potential is established by an entirely gaseous phase, CO/CO_2 mixture (say). The attack of $CaSO_4$ in low oxygen potential established via CO_2/CO gas should be similar to that obtained in $CaSO_4$/C mixture if the function of the graphite is to merely maintain a low oxygen activity around the $CaSO_4$. Therefore, the use of more controlled atmosphere in investigating the effect of low oxygen activity on $CaSO_4$-induced corrosion is ideal and practical. In figure (13) are shown the optical

micrographs of the cross-sections of IN 800, Fe-20Cr and stainless steel 310 oxidised in $CaSO_4/CaO$ mixture at 850°C in low oxygen pressure of 10^{-19} atm. for 100 hours. The low oxygen pressure was fixed via CO/CO_2 mixture which was allowed through the test tube containing the samples and the $CaSO_4/CaO$ mixture for fifteen minutes. The depth of attack of the IN 800 was of the order 5×10^{-3} mm. Also, the thickness of the scales formed on stainless steel 310 and Fe-20Cr were of the order of 5×10^{-3} mm. There is no sulfidation in all cases. The scales in all three cases also contain small quantities of calcium. When compared with figures (8) to (10) where graphite is supposed to fix the low oxygen potential, the results of figures (13) suggest that it is not necessarily low P_{O_2} that causes the sulfidation attack of $CaSO_4$. From the Ca-O-S stability diagram, CaS and CaO are stable at P_{O_2} of 10^{-19} atm. Therefore, the three alloy samples were also oxidised in CaS/CaO mixture at the same P_{O_2} (10^{-19} atm.) for the same time (100 hours) with the same gas mixtures. Figure (14) shows the micrographs of their cross-sections. The attacks are very similar and the extent of oxidation is approximately the same. Also, there is no sulfidation. The similarity in the attacks of $CaSO_4/CaO$ and CaS/CaO is due to the fact that the reduction of $CaSO_4$ to CaS does not involve loss of sulfur.

The measured oxygen pressure of a typical fluidised-bed coal combustor operating with limestone addition at 850°C is the order of 10^{-12} atm. (see page 11). In figure (15) is shown the optical micrograph of the cross-sections of the scale formed on the three alloys (IN 800, Fe-20Cr, st. st. 310) after oxidation in $CaSO_4/CaO$ mixture at 850°C in a relatively higher oxygen pressure of $10^{-11.5}$ atm. for 100 hours. As before, the CO/CO_2 gas mixture was used in fixing the oxygen pressure, the flow being maintained for the first fifteen minutes of the total

100 hours of the tests. The IN 800 developed a depth of internal oxidation of the order of 10^{-2} mm at the sides, attaining a maximum value of 10^{-1} mm at the corners with occasional blisters on the main scale. Blistering of oxides is usually due to growth stress. There is no sulfidation. Fe-20Cr showed a completely detached main scale and there are no regions of internal attack. It is not certain whether the scales detached during cooling or during oxidation. Stainless steel also developed considerable internal penetration attack. In all three cases considered above, there is no sulfidation. With stainless steel 310 and IN 800, the regions of internal penetration attacks appear, at first, to resemble sulfides, but no sulfides were detected in Edax analysis. Also, in all three tests above, calcium peaks were detected in some regions of the scale particularly towards the surface. Iron peaks always appear with calcium suggesting the possibility of reaction between the iron oxide and the $CaSO_4$. In figure (16) is shown the scanning electron image and the X-ray maps of the simplest of the three alloys, Fe-20Cr after oxidation at P_{O_2} of $10^{-11.5}$. The calcium and iron maps correspond and there is little chromium in the detached portion of the scale. However, the adherent portion of the scale is mainly chromium oxide.

D. Effect Of Fixing Both P_{O_2} And P_{S_2} On $CaSO_4$-Induced Corrosion

In figures (17) is shown the cross-section of IN 800, oxidised for 100 hours in $CaSO_4$ salt at 850°C under a gas environment established by 3.5%H_2, 1%H_2S, bal. CO_2 gas mixture which was allowed to flow through for fifteen minutes. Assuming thermodynamic equilibrium is established, the gas mixture should correspond to 10^{-4} atm. of sulfur and 10^{-6} atm. of oxygen. The scale formed on IN 800 consists of non-adherent porous outermost scale. It is not certain whether the scale detached during cooling. However, the adhering portion of the scale appears to be mainly

regions of internal penetration attack consisting of irregularly shaped chromium sulfides. Further beneath, the chromium sulfides follow the grain-boundaries, keeping ahead of the oxidation front. The sulfides themselves oxidise, and the sulfur released can either diffuse further into the alloy forming sulfides, in which case the attack is self-propagating, or escape through the porous, non-adherent outermost scale, in which case the attack is self-limiting, and will slow down, unless there is a continuing supply of sulfur. Originally, it was thought that the removal of the chromium to form the sulfides allowed the rapid oxidation of the depleted matrix, but, in fact, it appears that the chromium-rich sulfides themselves oxidise rapidly, forming a layer in which particles of metal depleted in chromium are embedded in a non-protective chromium oxide matrix. Eventually, towards the outer part of the scale the particles of relatively noble metal oxidise. In other cases, the sulfur activity can rise sufficiently high so that sulfides of the more noble metals form, and these may be liquid, e.g., NiS at $850^{o}C$. The appearance of a liquid phase within the metal appears to result in accelerated breakdown, the liquid phase penetrating rapidly along the grain-boundaries. The depth of penetration of the zone of internal attack is about 0.4 mm.

In figure (18) is shown the cross-section of Fe-20Cr oxidised under the same conditions as that of figure (17). Fe-20Cr amassed a considerably bigger scale, but it is detached from the alloy. Again, it is not known whether the detachment occurred during cooling or oxidation. There is sulfidation confined to the interface between the adhering portion of the scale and the unattacked matrix. The thickness of the external scale is about 0.3 mm. The main detached scale consists of two regions, an innermost layer containing chromium and iron and an outermost region

consisting mainly of iron and calcium oxide with very little chromium. The adhering portions of the scale is mainly chromium oxide. Therefore, the effect of fixing both oxygen and sulfur partial pressures is to cause increase in the rate of $CaSO_4$-induced oxidation and sulfidation. In addition, the $CaSO_4$ was molten after the tests of figures (17) and (18). Thus it appears that high partial pressures of sulfur lower the melting point of $CaSO_4$. It is also possible calcium pyrosulfate, CaS_2O_7, is formed and then melts.

E. Effect of NH_3

NH_3 is among the gases that are given off during the combustion of coal, although the exact percentage in the case of the fluidised-bed combustor is yet to be determined and measured. However, NH_3 can be present as a micro-component in the gas phase to the extent that it could possibly affect the equilibrium of the $CaSO_4$-containing deposit. In figure (19) are shown the cross-sections of IN 800, and stainless steel 310 oxidised in $CaSO_4$ salt and $(NH_4)_2CO_3$ vapor at 850°C for 60 hours. The ammonium carbonate has a melting point of less than 100°C, thus, by introducing a small quantity of $(NH_4)_2CO_3$ into the horizontal furnace containing the sample and the $CaSO_4$ at 850°C, the ammonium carbonate will evaporise mainly as NH_3 and CO_2 gases which then sweep across the crucible containing the specimens and $CaSO_4$. Internal sulfides are present as the Edax result suggests and furthermore, there is significant internal penetration attack in both IN 800 and stainless steel 310. Also, there is no marked detachment of the main scale, although there is quite considerable porosity within the main scale which sometimes border on near-complete detachment.

F. Effect Of Temperature On $CaSO_4$-Induced Corrosion

There are local hot regions within the fluidised-bed. Temperatures are known to differ by as much as 200°C. To investigate the effect of temperature on the $CaSO_4$-induced attack, consider figures (20) which show cross-sections of IN 800, stainless steel 310 and Fe-20Cr oxidised embedded in $CaSO_4$ at 1100°C for three hours in static air. The scale formed on IN 800 consists of an outermost detached scale and a porous, loosely adhering inner scale. There is also a zone of internal oxidation/sulfidation confined along the grain-boundaries. The presence of the internal sulfides along the grain-boundaries automatically exposes this alloy to catastrophic attack, i.e., the CrS - Cr_2O_3 cycle. The porous loosely adherent portion of the scale consists of pockets of oxides of particles of relatively noble metals, chromium oxide, chromium sulfides, nickel oxides, iron and calcium oxide. The outermost detached scale consists of mixtures of iron oxide and some calcium sulfate.

Fe-20Cr at 1100°C developed a considerably thicker scale, about 0.6 mm. The scale consists of mixtures of oxides and sulfides of iron, and chromium with some CaO and $CaSO_4$. The dendritic appearance of the scale on Fe-20Cr suggests the possibility of a liquid phase.

Stainless steel on the other hand was relatively mildly attacked. Evaporation reaction appears to have taken place in the regions in which the stainless steel was attacked. Grooves penetrating to a depth of about 2.5×10^{-2} mm below the surface can be seen in the cross-section. Connecting these grooves to the interior of the matrix are grain-boundary attacks. Chromium sulfide was identified along the grain-boundaries. At 1100°C, the $CaSO_4$ apparently decomposes, providing sufficient sulfur to form NiS and which is liquid. CrS and Cr_2O_3 will also form as well as the volatile phase of chromium oxide. The presence of these volatile

and liquid phase accounts for the loss of material inside the grooves. Under the above circumstances, the attack will tend to be catastrophic with time.

In figures (21) are shown the cross-sections of stainless steel 310, Fe-20Cr, and IN 800 oxidised in $CaSO_4$ depost at 1050^oC for twenty hours in static air. Stainless steel at lower temperature, 1050^oC and longer time, developed relatively thick scale, about 2.5×10^{-2} mm thick. The scale appears very porous. Cracks run through the scale, connecting the grain-boundary attack within the matrix. The depth of the maximum penetration of the grain-boundary attack is about 5×10^{-2} mm. Chromium can be identified along the grain-boundaries. Oxides of nickel and iron are present in the main scale, but the main component is chromium oxide. Chromium sulfides are also present within some of the cracks that run through the main scale. It appears that within these cracks, pockets of isolated gas were depleted in oyxgen causing the sulfur partial pressure to drastically increase. NiS can form and at 1050^oC is liquid. The liquid phase will thus enhance the propagation of the crack right into the alloy matrix. The cracks in the first place can be caused by sheer stresses due to the growth stress. On cooling, the NiS reacts with Cr_2O_3 forming NiO and CrS.

Fe-20Cr at 1050^oC developed a scale of about 1 mm thickness. The main scale is made up of a mixture of sulfides and oxides of iron and chromium as well as calcium sulfate and calcium oxide. There is no internal oxidation or sulfidation. The scale/alloy interface is smooth. The upper-most portion of the scale is detached. It is not certain whether this detachment took place during cooling or oxidation.

Stainless steel 310 at 1050^oC, had quite considerable internal attack that does not necessarily follow the grain-boundaries but appears

as elongated spikes. Some of these spikes are aluminum and chromium oxides although in some places, chromium sulfide can be identified. The upper adhering scale is very porous and is made up of Cr_2O_3, NiO, FeO and some calcium sulfate. Directly beneath the main scale, extending about 7×10^{-3} mm inwards is a zone of CrS.

The $CaSO_4$-induced corrosion at 1100°C and 1050°C contrasts very sharply with those at lower temperatures. At 950°C and below, the $CaSO_4$-induced attack in static air and in controlled sulfur-free bulk atmosphere, does not involve sulfidation while at 1050°C and 1100°C, the $CaSO_4$-induced corrosion generally involves sulfidation. Also, a strong temperature dependence is shown by graphite-containing $CaSO_4$: at 950°C, for instance, Fe-20Cr after oxidation in $CaSO_4$/C in static air for twelve hours, suffered sulfidation attack right around and beneath the main scale while at 850°C, and under the same condition, Fe-20Cr after 100 hours suffered sulfidation at only one region - beneath the entire main scale (see figures (8), (9) and 12)).

CHAPTER 3: MECHANISM(S) AND CONCLUSIONS

The summary of the results presented above indicate that $CaSO_4$ is capable of inducing unacceptable corrosion of iron-based materials employed in fluidised-bed coal combustors operating with limestone or dolomite additions.

At constant temperature, for instance 850°C, the $CaSO_4$-induced corrosion of incoloy 800, stainless steel 310 and Fe-20Cr increases with increasing oxygen activities (see table below). The increase in $CaSO_4$-induced corrosion with increase in oxygen activity is contrary to the earlier expectation that the $CaSO_4$-induced attack should depend only on the sulfur activity according to the Ca-O-S stability diagram, figure (2), (c.f see chapter on objectives).

A. $850^{o}C\text{-}CaSO_4/CaO + P_{O_2} = 10^{-19}$ atm. (100 hrs.)

	Depth Of Internal Attack (mm) (Average)	Thickness Of Main Scale (mm) (Average)	Sulfide Attack?
IN 800	5×10^{-3}	--	No
Fe-20Cr	--	5×10^{-3}	No
St. St. 310	--	5×10^{-3}	No

B. $850^{o}C\text{-}CaSO_4/CaO + P_{O_2} = 10^{-11.5}$ atm. (100 hrs.)

	Depth Of Internal Attack (mm) (Average)	Thickness Of Main Scale (mm) (Average)	Sulfide Attack?
IN 800	10^{-2} -- 10^{-1}	4×10^{-3} (detached)	No
Fe-20Cr	--	2.4×10^{-2}	No
St. St. 310	5.8×10^{-2}	2.5×10^{-2}	No

At all oxygen pressures, the main scale contains calcium, the relative amount of which increases with increasing $^{P}O_2$ and corresponds also to increasing overall attack by the $CaSO_4$. It appears the $CaSO_4$/ oxide interaction is associated with the frequent loss of adherence by the scale. Furthermore, the occurence of calcium within the scale does follow a certain pattern: iron peaks are always picked up along with calcium peaks in all Edax analysis, thereby suggesting the possibility of a solid state reaction between the two (calcium and iron oxide).

In mixed gases of oxygen and sulfur with high sulfur and oxygen activities (10^{-6} atm. $^{P}O_2$ and 10^{-4} atm. $^{P}S_2$ at 850°C), IN 800 suffered considerable sulfidation attack in $CaSO_4$ deposit after 100 hours, the overall attack consisting of a non-adherent porous outermost scale (figure 17) and an adhering portion of the scale which consists mainly of regions of internal sulfidation. The internal sulfides run along the grain-boundaries, penetrating to a depth of about 0.4 mm below the main scale. Fe-20Cr in $CaSO_4/^{P}O_2/^{P}S_2$ environment also suffered considerable attack consisting of relatively thick scale ~ 0.3 mm, with limited sulfidation along the scale/alloy interface, i.e., ahead of the oxidation front. stainless steel 310 in $CaSO_4/^{P}O_2/^{P}S_2$ environment suffered only considerable oxidation and no sulfidation. Presence of calcium within the scale was observed in all three cases, with relatively high iron peaks occurring with the calcium peaks during the Edax analysis. Furthermore, at this high $^{P}O_2 = 10^{-6}$ atm. and $^{P}S_2 = 10^{-4}$ atm. (850°C), the $CaSO_4$ appeared molten after the test. The attack of $CaSO_4$ in high oxygen and sulfur activities correspond to the case where the addition of the CaO into the fluidised-bed coal combustor is not continuous in which case the unreacted CaO would have all reacted to form $CaSO_4$. Thus, the sulfur activity within the bed will revert to its pre-dolomite-addition value.

The sulfidation attack observed after oxidising In 800 and Fe-20Cr in $CaSO_4$ deposit under a sulfur activity of 10^{-4} at 850°C is largely due to the sulfur in the gas and not the $CaSO_4$ deposit; for instance, all samples oxidised in $CaSO_4$ and in sulfur-free bulk gases did not suffer sulfidation at 850°C (see figures 13 & 14).

With graphite additions to $CaSO_4$ in static air, the $CaSO_4$-induced attack involves sufidation at 950°C, but the rate of sulfidation decreases with decreasing temperature. Therefore, the mechanism by which the graphite induces the $CaSO_4$ to decompose is temperature-sensitive. Also, at a fixed temperature, the rate of sulfidation and oxidation of IN 800, Fe-20Cr and St. St. 310 in a $CaSO_4$/C deposit decreases with increasing exposure time. It appears, the graphite and the $CaSO_4$ become depleted with time.

However, when ammonia gas is passed through $CaSO_4$ in static air (850°C), the $CaSO_4$-induced attack involves sulfidation. Below is shown a table of comparison between the sulfidation effects of graphite and ammonia gas when they are contained in $CaSO_4$ deposit in static air. The parameters are depth of internal sulfide penetration below the main scale and maximum thickness of main scale.

Alloy	Maximum Depth of Sulfidation		Maximum Scale Thickness	
	NH_3 (60 hrs.)	C (100 hrs.)	NH_3 (60 hrs.)	C (100 hrs.)
	(mm)	(mm)	(mm)	(mm)
IN 800	8×10^{-2}	7×10^{-2}	1.1×10^{-2}	1.25×10^{-2}
St. St. 310	4×10^{-2}	2.5×10^{-2}	3×10^{-2}	8×10^{-3}

It appears the NH_3 acts as a strong reducing agent for the $CaSO_4$. The effects of NH_3 and graphite in $CaSO_4$-induced sulfidation/oxidation as

shown above, at first can be misleading: in $CaSO_4/NH_3$ case, the sulfidation attack was generally uniform at 850°C, while in the case of $C/CaSO_4$, the sulfide regions are confined to one or two locations and in most cases appear hard to detect (figure 12). Also, the test in $C/CaSO_4$ lasted longer than the $CaSO_4/NH_3$ test at 850°C in static air. However, at 950°C, graphite/$CaSO_4$ sulfidation becomes marked and uniform. The sulfidation usually follows grain-boundaries.

With temperature as the only variable, and in static air, the $CaSO_4$-induced attack increases with increasing temperature. At 950°C and below, $CaSO_4$-induced attack does not involve sulfidation. Only direct reaction between the oxide and the salt is observed and which relates to the calcium within the scale. Also, in all cases, where there was no sulfidation (950° and below), the main scale consists of a mixture of oxides, with Cr_2O_3 often predominant. The table below shows the types of oxides comprising the main scale of IN 800, Fe-20Cr and stainless steel 310 after oxidation in $CaSO_4/P_{O_2} = 10^{-11.5}$ atm. at 850°C.

	Types of Oxides in the Main Scale (In Order Of Increasing Amount)			
IN 800	Cr_2O_3	FeO	Cr_2O_3	CaO
Fe-20Cr	FeO	CaO	Cr_2O_3	
St. St. 310	Cr_2O_3	FeO	NiO	CaO

Thus, it appears the $CaSO_4$/ oxide interaction alters the stability or kinetics of the different oxides present within the scale, substantially favoring iron migration and hence incorporation into the scale. At temperatures greater than 950°C, $CaSO_4$-induced attack involves sulfidation, the

attack decreasing with time possibly due to depletion of $CaSO_4$. The extent of attack on st. st. 310 is always the least.

Temperature effect as the only variable in $CaSO_4$-induced attack is particularly severe above 1000°C. IN 800, Fe-20Cr and stainless steel 310 when oxidised in $CaSO_4$ in static air, develop scales which appear to have been molten during exposure (see figure 20 and 21). The scale formed on Fe-20Cr when oxidised in $CaSO_4$ deposit in static air at 1100°C had dendritic appearance, possibly developed during cooling of the molten scale, while stainless steel 310 developed grooves which are possibly related to evaporation reaction. In the case of stainless steel, as mentioned previously, the evaporation reaction may be linked to the formation of the volatile chromium oxide or liquid nickel sulfide. Liquid or molten phase attack once present during corrosion invariably leads to catastrophic attack, often involving grain-boundary crack and subsequent liquid penetration.

From the experimental results, it appears $CaSO_4$-induced attacks fall into two main categories:

1. Solid-state attack involving calcium and iron or iron oxide mainly.
2. Liquid phase attack.

The two modes of attacks above have one common characteristic: regions within the main scale containing calcium also have relatively high iron contents than regions where there are no calcium (see for instance figure (16). Therefore, the attack of iron by $CaSO_4$ needs to be investigated to establish the possible mechanisms involved. First of all, it has to be established that it is iron oxide that interacts with the calcium and not any other oxides present within the scale. In figure (22) are shown cross sections of the scale formed on pure iron, nickel and chromium after oxidation for (11) hours in $CaSO_4$/C deposit at 850°C in static air. The

pure chromium is relatively resistant, forming a continuous Cr_2O_3 scale of about 2.5×10^{-3} mm thick. There is no scale on the pure nickel after similar oxidation, rather rugged, protruding unattacked nickel matrix mark the interface between the $CaSO_4$/C deposit and the initial nickel. NiS frequently is seen cutting right through the base of a protruding unattacked nickel matrix. Since NiS is liquid at 850°C, this means the protruding matrix will shear off at the base where the liquid NiS is formed. In this way, the pure nickel matrix loses its grains. Therefore Ni does not appear to interact with the $CaSO_4$ salt, but if the $CaSO_4$ is induced to decompose and release Sulfur, NiS and NiO will be formed and at 850°C, NiS is liquid, thus leading to the bulk metal loss.

Pure Iron after oxidation in $CaSO_4$/C deposit at 850°C in static air for (11) hours developed relatively thick porous mixed scale, consisting of FeS, iron oxide and calcium. Therefore, pure iron and hence its oxide interacts strongly with $CaSO_4$ deposit. Pure chromium is resistant to direct $CaSO_4$ attack, while nickel is susceptible only if sulfidation is involved.

The chemical analysis of the calcium/iron oxide interaction was investigated by oxidising pure iron embedded in $CaSO_4$ at 10^{-17} atm. P_{O_2} for four hours, the resulting scale was crushed and analysed using the Debye-Scherrer powder method. The calcium-iron compound has the chemical formula $CaFeO_2$ and the crystals are rounded under the microscope. It is cubic with unit cell length of 4.762Å. $CaFeO_2$ consists of 72.6% CaO, 21.99% FeO and 4.9% Fe_2O_3 [10].

To study the interaction between the $CaSO_4$ and the iron and/or iron oxide, a hole 0.131 inches was drilled in a 1.25 x 0.156 o.d. cylinderical pure iron and $CaSO_4$ was packed into the hole. The iron-$CaSO_4$ assembly was oxidised in air between 850°C and 950°C in a hot stage micro-

scope evacuated to 10^{-5} atm. total pressure. In figure (23) are shown the micrographs of the cross-sections of the $CaSO_4$/iron interface during different periods of the test. The micrographs in figure (23) are numbered 'A', 'B' ... 'E'. Time and temperature are continuously monitored and are recorded on the bottom right-hand side of each picture. 'A' shows the top view of $CaSO_4$/iron assembly at room temperature. The white shiny central region is the $CaSO_4$ contained in the hole and the very dark, immediately adjoining region, is the iron matrix. The $CaSO_4$/ iron interface shown by the white arrow is enlarged in 'B'. Again the white and dark regions are the $CaSO_4$ and the pure iron matrix. As the temperature is increased, there is local re-arrangement of the $CaSO_4$ salt possibly as a result of sintering and the pure iron matrix becomes lighter in color due to increase in conductivity. Above $800^{o}C$ (see 'C') a crack or partition is suddenly developed at a point within the $CaSO_4$ and near the $CaSO_4$/iron oxide interface. This crack propagates leaving some of the $CaSO_4$ attached to the FeO-since oxidation must have occurred. Two stages during the detachment are shown by 'C' and 'D'. In some places (see 'E') the $CaSO_4$ attacked dug deeper into the iron oxide regions towards the iron matrix. At the end of the test, the sample was analysed under the scanning electron microscope In figure (24) are shown the scanning electron image and X-ray maps of a section through the $CaSO_4$/ iron oxide after the hot stage experiment.

As regards the relative positions of the $CaSO_4$ and the iron matrix: the black region tracing out a curve about the top left-hand corner of the scanning electron image defines the partition or the crack profile whose method of propagation is the same as those already shown in 'C' and 'D' of figure (23) respectively. The crack or partition in figure (24) occurred after those of figure (23), this time serving to detach the product

of reaction between the $CaSO_4$ and the iron oxide. The X-ray maps of figure (24), indicate Iron migrated out into the $CaSO_4$. The sulfur level or amount in the region where calcium, iron and sulfur occur together is significantly less than its level in the region where only calcium and sulfur occur together. Evidence that iron oxide grows out towards the $CaSO_4$ or the calcium can be seen in the scanning electron image of figure (23): finger-like out-growths can be seen deep along the void and X-ray map of iron indicates these protrusions are iron oxides. Therefore, iron on diffusing out, forms iron oxide which tends to grow directionally towards the $CaSO_4$. The resulting reaction between iron oxide and $CaSO_4$ yields a non-adherent scale, which in time will detach. It, thus, appears the reaction between iron oxide and $CaSO_4$ produces sulfur, or rather, releases sulfur because, the region where calcium, iron oxide and sulfur occur contains significantly less sulfur than that associated with $CaSO_4$.

To investigate the stability of the product phase of $CaSO_4$/iron reaction, a section of the interface with a rounded scale was selected. The temperature was increased and the behavior of the scale was monitored continuously by the video camera. In figure (25) are shown the stage-by-stage demonstration of the recorded reaction that took place during the increase in temperature. Again, the temperature and time are shown on the bottom right-hand corners of each micrograph. The scale melted forming a pool. The melting started at about 927^{o}C & at 957^{o}C, only pool of liquid marked the position of the rounded scale. In addition, the region on the top left-hand corner of figure (25) also melted and it is $CaSO_4$, possibly with some iron contaminations. However, this motion picture demonstrates vividly that a liquid phase attack does, indeed, occur and is involved in $CaSO_4$-induced attack at high temperature provided iron is present, For pure Iron in $CaSO_4$ deposit, the onset of the liquid phase is about 927^{o}C.

To isolate the molten phase in the iron/$CaSO_4$ reaction, a pure iron sample was oxidised in $CaSO_4$ deposit at 1100°C for two hours, in static air. At the end of two hours, the crucible containing the iron and $CaSO_4$ was quickly withdrawn. A molten pool was observed in place of the pure iron sample and the covering $CaSO_4$. In figure (26) is shown the scanning electron image of the molten phase after cooling. Edax analysis shows the protruding light regions of figure (26) contain Ca, Fe, S_2, while the dark regions contain mainly smaller amounts of Ca and Fe. The chemical analysis result of the molten compound formed from the $CaSO_4$/iron reaction after solidifying as computed by Annamet Laboratories is shown below:

CHEMICAL ANALYSIS

Calcium	(Ca)	30.8%
Iron	(Fe)	36.3%
Oxygen	(O)	29.0%
Sulfur	(S)	5.75%

Two possible formulae, or empirical formulae are as follows:

$$3CaO \cdot 3FeO \cdot CaSO_4$$

Or

$$4CaO \cdot 2FeO \cdot FeSO_4$$

Therefore, the possible mechanism(s) of the attack of iron by $CaSO_4$ involves first the formation of iron oxide, in the presence of oxygen. The iron oxide grows directionally, as spikes, towards $CaSO_4$ deposit. The iron-oxide reacts with the $CaSO_4$ releasing sulfur and forming $CaFeO_2$. The $CaFeO_2$ is sulfidised by the sulfur gas, requiring lesser amount of sulfur than $CaSO_4$/FeO reaction had made available. The above reactions may be

represented by the following equations:

$$Fe + \tfrac{1}{2}O_2 = FeO \qquad (1)$$

$$FeO + CaSO_4 = CaFeO_2 + SO_3 \qquad (2)$$

Direct evidence that the iron oxide locally induces the decomposition of the $CaSO_4$ is presented in figure (27) and shows the top view of the part of the $CaSO_4$ immediately bordering the scale. Unlike the white color of $CaSO_4$ in the regions away from the scale/$CaSO_4$ interface, the $CaSO_4$ bordering the scale is yellowish in color. In figure (27), the scale has been removed exposing the $CaSO_4$ bordering it. The black areas are particles of iron oxide. The thickness of this yellowish layer is very small and very difficult to measure quantitatively. PH measurements of the yellowish layer were taken and compared with that of ordinary $CaSO_4$, i.e., unused $CaSO_4$ together with that of a region away from the yellowish layer. The results are presented below:

	pH (measured)
Unused $CaSO_4$	6.2
Used $CaSO_4$ - not yellowish	6.45
Used $CaSO_4$ - yellowish	7.3

(Above pH values are relative)

Finally, weight gain versus time measurements were conducted to further verify that the $CaSO_4$-induced attack at 850°C in sulfur-free bulk gases, i.e., CO/CO_2 increases with increasing $^{P}O_2$. In figure (28) are shown the weight gain versus time curves for pure iron when coated with $CaSO_4$ and oxidised in various oxygen pressures at 850°C. The break in the initial parabolic

curves occur at about the first 50 - 60 minutes of exposure, thereafter, the curves swing upward to higher weight gain values, while still maintaining parabolic rates. Initially, FeO is formed and its growth rate is parabolic and corresponds to the early parabolic curve. The break in the initial parabolic curve is associated with the sudden formation of $CaFeO_2$ and the subsequent reaction rate is determined by the kinetics of $CaFeO_2$ growth. The upward swing of the curve indicates $CaFeO_2$ is less protective than FeO and experimental results have confirmed the $CaFeO_2$ scale is, indeed, unprotective. The occurrence of $CaFeO_2$ within the outermain scale results in a layered scale with iron oxide usually found beneath the $CaFeO_2$ outer layer. Also, the shape of all the curves suggest the attack of iron by $CaSO_4$ once initiated occurs very quickly at first, the rate diminishing with time and this is consistent with all the results obtained previously. The occurrence of $CaFeO_2$ within the outermain scale results in a layered scale with iron oxide usually found beneath the $CaFeO_2$ outer layer. In figure (29) is shown the scale formed on pure iron after oxidising in $CaSO_4$ deposit for three hours in $^{P}O_2 = 10^{-19}$ atm. The layered morphology of the scale can be seen in figure (29) and the complex iron-calcium-sulfate occur as very thin layer above the $CaFeO_2$. During oxidation the complex calcium iron sulfate does not increase in thickness with time, but becomes liquid at high temperature thereby initiating catastrophic attack.

Essentially, this project has demonstrated that $CaSO_4$-induced attack of iron-based materials and especially pure iron can be catastrophic, involving:

(a) solid state reaction, or direct attack by $CaSO_4$;

(b) liquid-phase attack at $927^{o}C$ and above (pure iron).

Furthermore, the $CaSO_4$-induced attack is sensitive to oxygen and sulfur activities, carbon or graphite contaminants, NH_3 containing environment and temperature; all except oxygen cause sulfidation in some cases.

Future Work

Further studies will concentrate on: (1) phase studies of Ca-Fe-O-S system and (2) the effect of packing density of the $CaSO_4$ deposit on $CaSO_4$-induced corrosion. This will involve pore size distribution studies. In this regard, the pore size distribution will be time dependent. Also, $CaSO_4$ deposit-induced corrosion will be compared with corrosion under an inert deposit.

REFERENCES

1. Mesko, J. E., "Materials For Direct Combustion, Fluidised Bed, Steam Generators", Metal Progress, July 1977, pp 29-34.

2. Stringer, J. and Ehrlich, S., "High temperature Corrosion In Fluidised Bed Combustors", paper presented at ASME Annual Meeting, December 5, 1976.

3. Rogers, E. A., et al, "The Corrosion Performance Of Heat Exchanger Alloys In Fluidised Combustion Systems", paper at Eurocor International Corrosion Conference, London, September, 1977.

4. Stringer, J., "High Temperature Corrosion In Fluidised Bed", Ash Deposits And Corrosion Due To Impurities In Combustion Gases., Hemisphere Publishing Corporation, 1977.

5. Whittle, D. P., et al, "The High Temperature Oxidation of CO-Cr-Al Alloys Containing Yttrium Or Hafnium Additions", Thin Solid Films 45, 1977, pp 377-384.

6. Whittle, D. P., Akuezue, H. C., Allam, I. M., "The Influence Of Small Platinum Additions On Al_2O_3 Scale Adherence", LBL-9180, May 1979 (submitted to Oxidation of Metals).

7. Cooke, M. J., et al, "Oxygen Measurements In Flue Gases With A Solid Electrolyte Probe", Journal of Institute of Fuel, March 1972, pp 153-156.

8. Whittle, D. P., and Stringer J., (unpublished results) see preliminary data in Proceedings International VGG Conference on Corrosion and Deposits in Power Plants, Essen, June 1977.

9. Stringer, J., (private communication).

10. U.S. Steel Fundamental Research Laboratory.

TABLE 1

ALLOY	PROBABLE USE	COMPOSITION										
		Ni	Co	Cr	Fe	Al	Ti	Mo	W	Cb	Zr	C
SS 304	NONTURBINE	10	--	20	BAL	--	--	--	--	--	--	0.05
SS 309	NONTURBINE	14	--	23	BAL	--	--	--	--	--	--	0.05
SS 310	NONTURBINE	20	--	25	BAL	--	--	--	--	--	--	0.05
SS 316	NONTURBINE	10	--	18	BAL	--	--	2.5	--	--	--	0.05
SS 330	NONTURBINE	35	--	19	BAL	--	--	--	--	--	--	0.05
SS 333	NONTURBINE	48	3	25	18	--	--	3	--	--	--	0.05
SS 446	NONTURBINE	0.7	--	25	74	--	--	--	--	--	--	0.10
INCONEL 600	NONTURBINE	76	--	15.5	8.0	--	--	--	--	--	--	0.08
INCONEL 601	NONTURBINE	61	--	23	14.1	1.35	--	--	--	--	--	0.05
INCONEL 690	NONTURBINE	60	--	30.0	9.5	--	--	--	--	--	--	0.03
INCONEL 706	NONTURBINE	42	--	16	40	0.20	1.75	--	--	--	--	0.03

TYPICAL CORROSION-TEST CANDIDATE MATERIALS

TABLE 2

ALLOY	TEMPERATURE, °F				
	752	932	1112	1292	1562
MEDIUM CARBON STEEL	20	40	--	--	--
2¼% Cr-1% Mo	20	40	270	--	--
12% Cr (410)	1	2	2	4	320
316	1	1	2	7	13
347	1	1	1	5	--
ESSHETE 1250	1	1	3	9	14
NIMONIC PE16	--	--	--	3	5

WEIGHT LOSS DATA (mg/cm^2) FOR ALLOYS EXPOSED FOR 1000 HOURS IN FBC (NCB-EPA 1971) (SPECIMENS DESCALED BEFORE BEING WEIGHED)

FIGURE 1

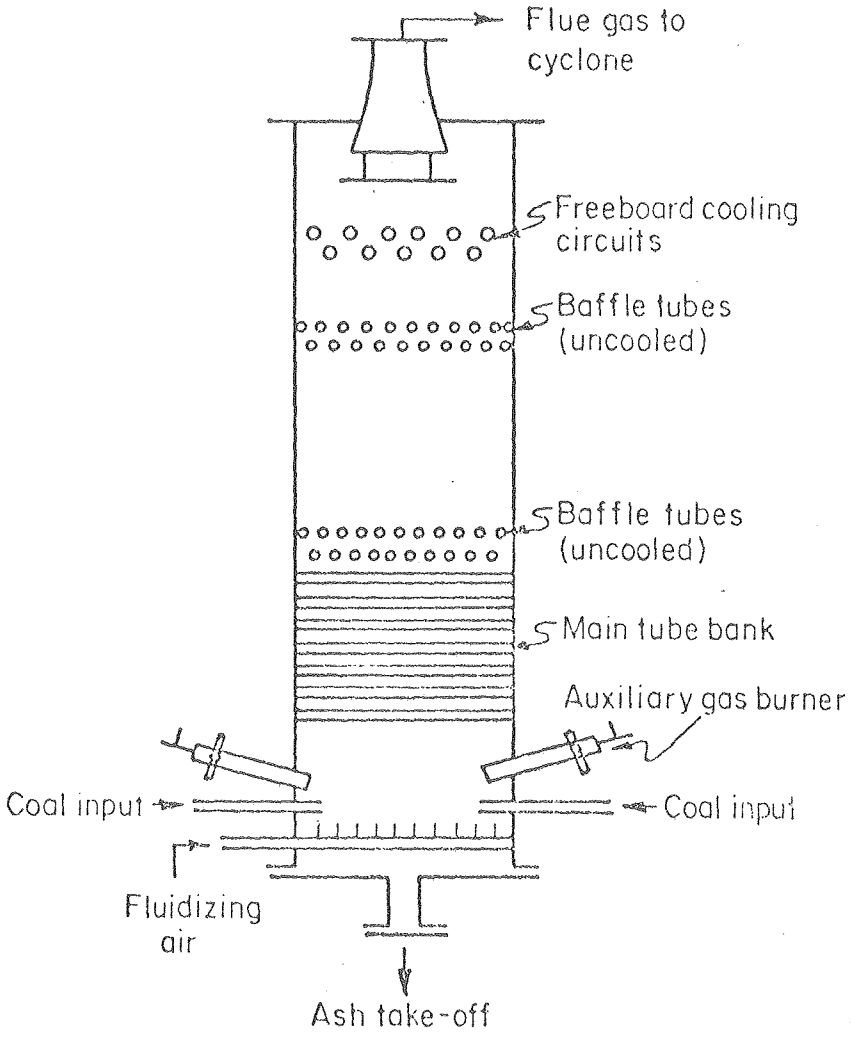

SCHEMATIC DIAGRAM OF A FLUIDIZED BED COMBUSTOR

XBL 796-10096

FIGURE 2A

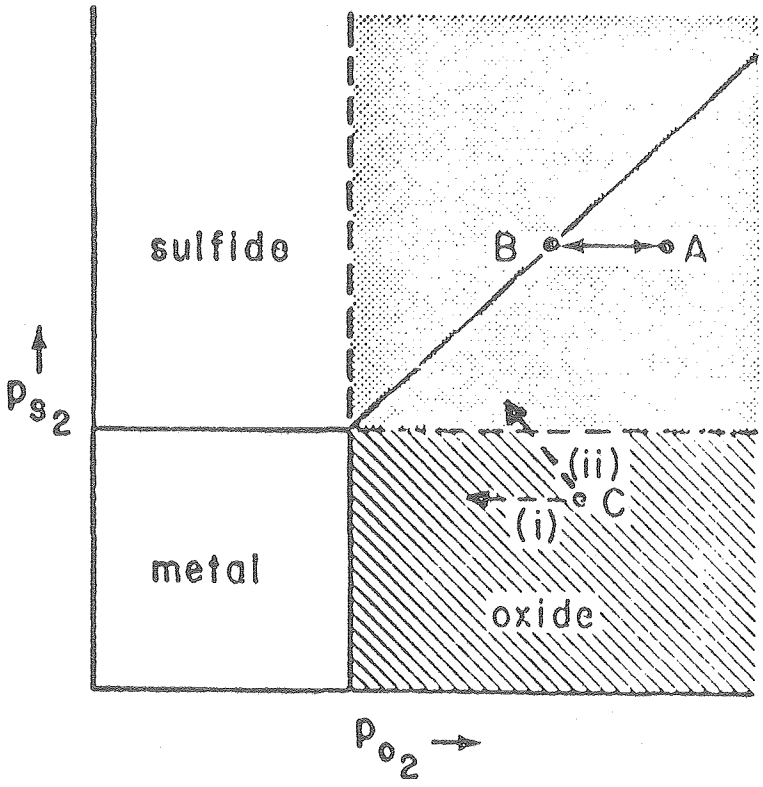

SCHEMATIC M-S-O STABILITY DIAGRAM SHOWING THE AREAS OF ACTIVITIES REFERRED TO IN THE TEXT

XBL 7911-12896

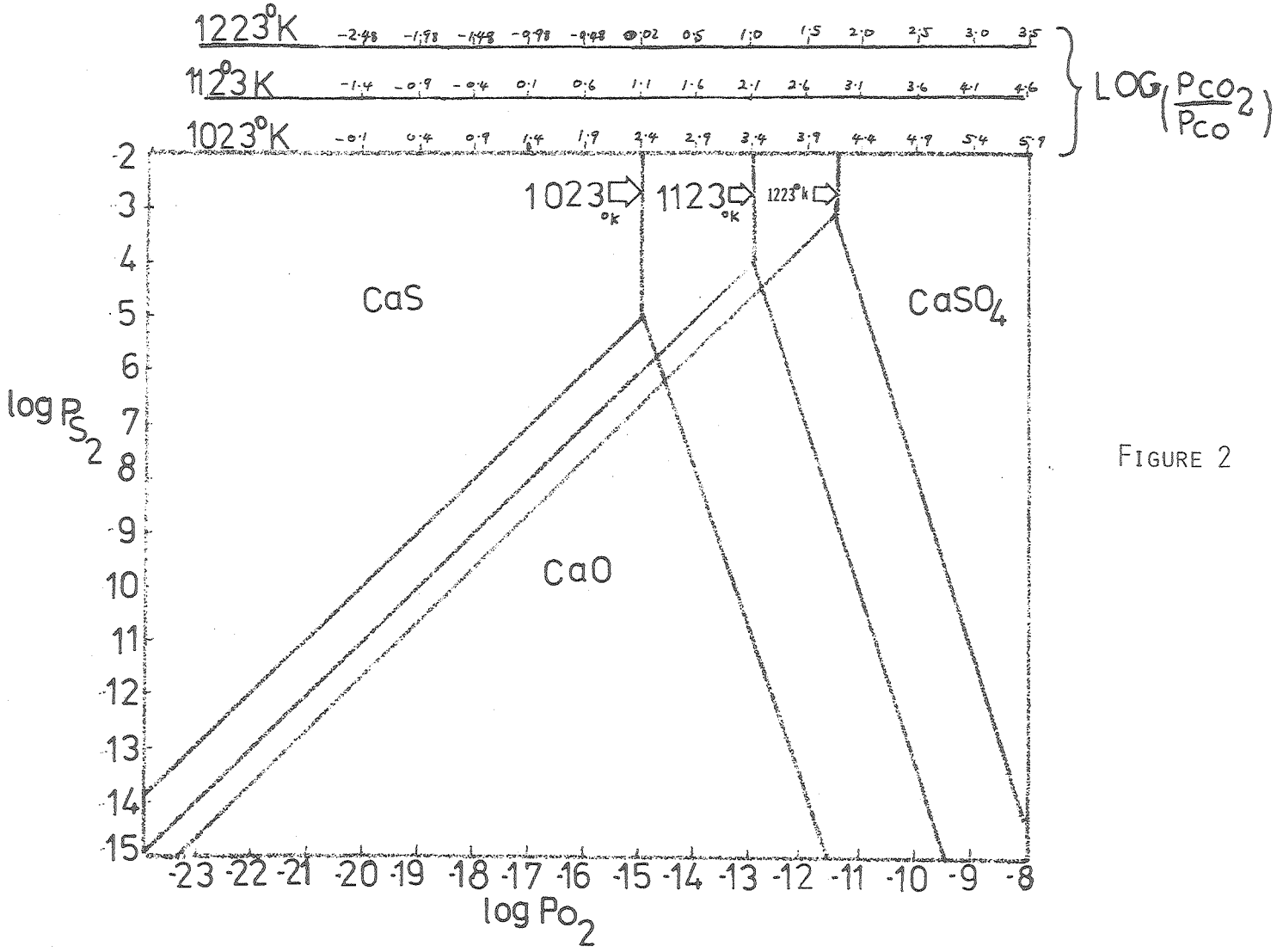

FIGURE 2

Phase stability diagram for the system Ca-S-O for 3 temperatures.

XBL 7911-12794

FIGURE 3

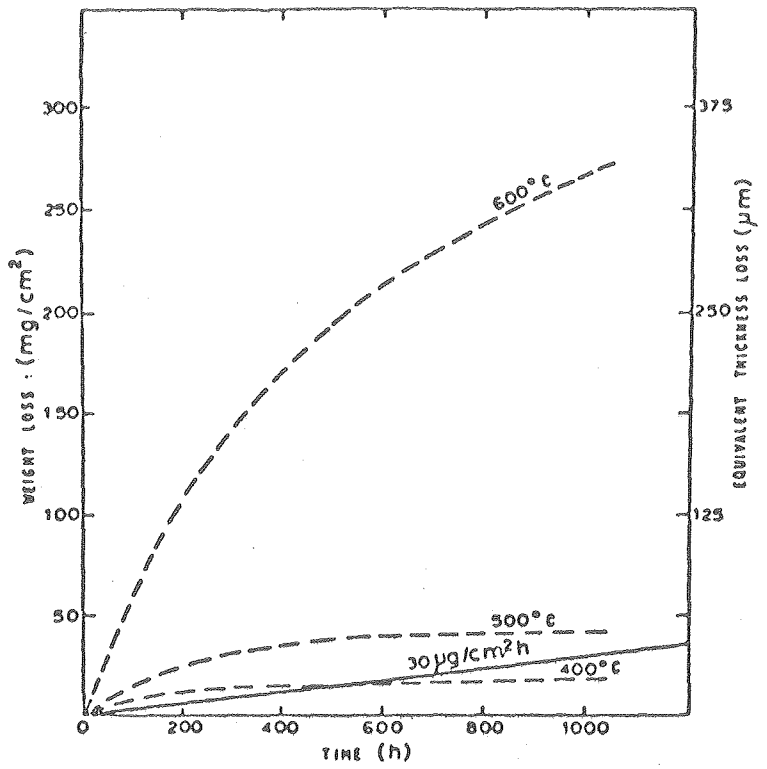

Descaled weight loss as a function of exposure time in a fbc for low-chromium steels (1 Cr-1/2Mo; 2 1/4Cr-1Mo) (NCB-EPA, 1971) [2]

XBL 7911-12898

FIGURE 4

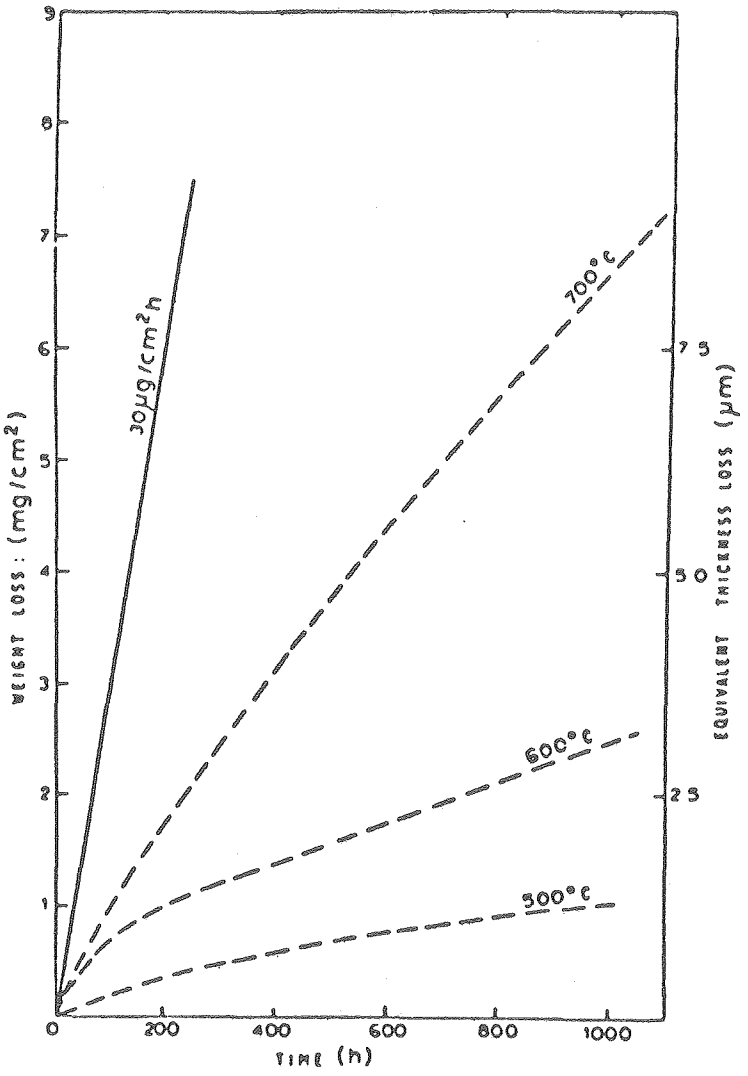

Descaled weight loss versus exposure time in a fbc for austenitic alloys (316, 347, Esshete 1250, Nomonic PE16 and 12Cr Steel) (NCB-EPA, 1971)[2]

XBL 7911-12897

FIGURE 5

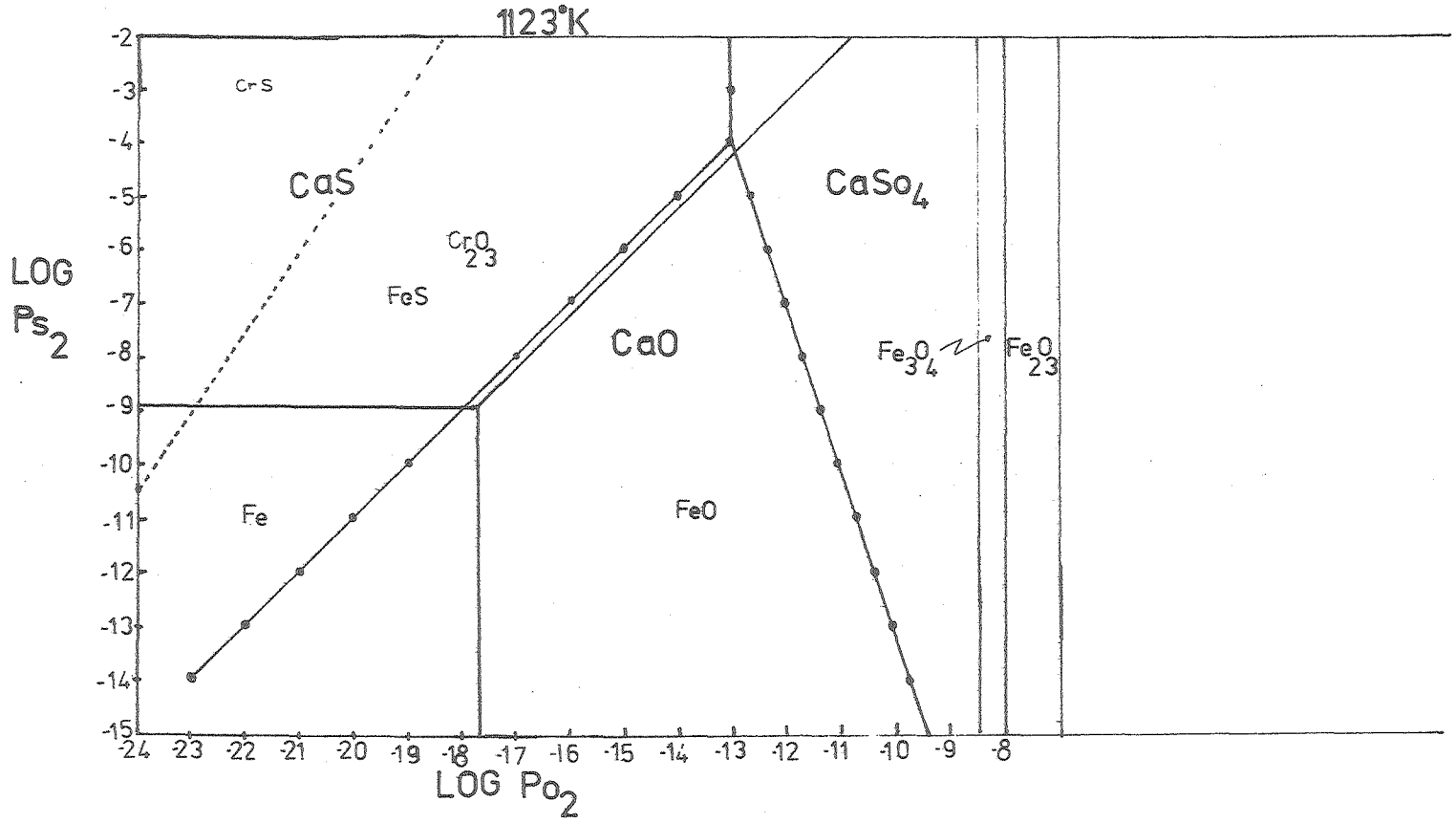

XBL 7911-12793

Fe-O-S and Cr-O-S stability diagrams superimposed on Ca-O-S stability diagram at 850°C.

FIGURE 6

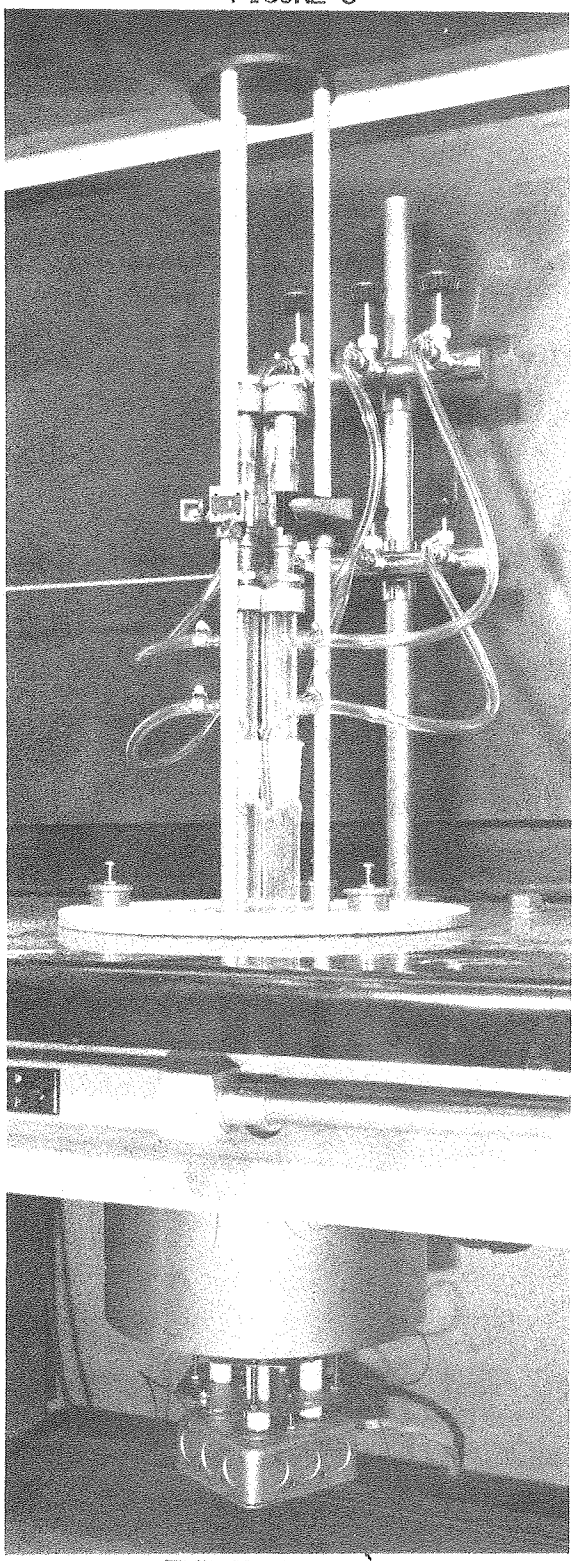

THE APPARATUS

XBB 781-776

FIGURE 7

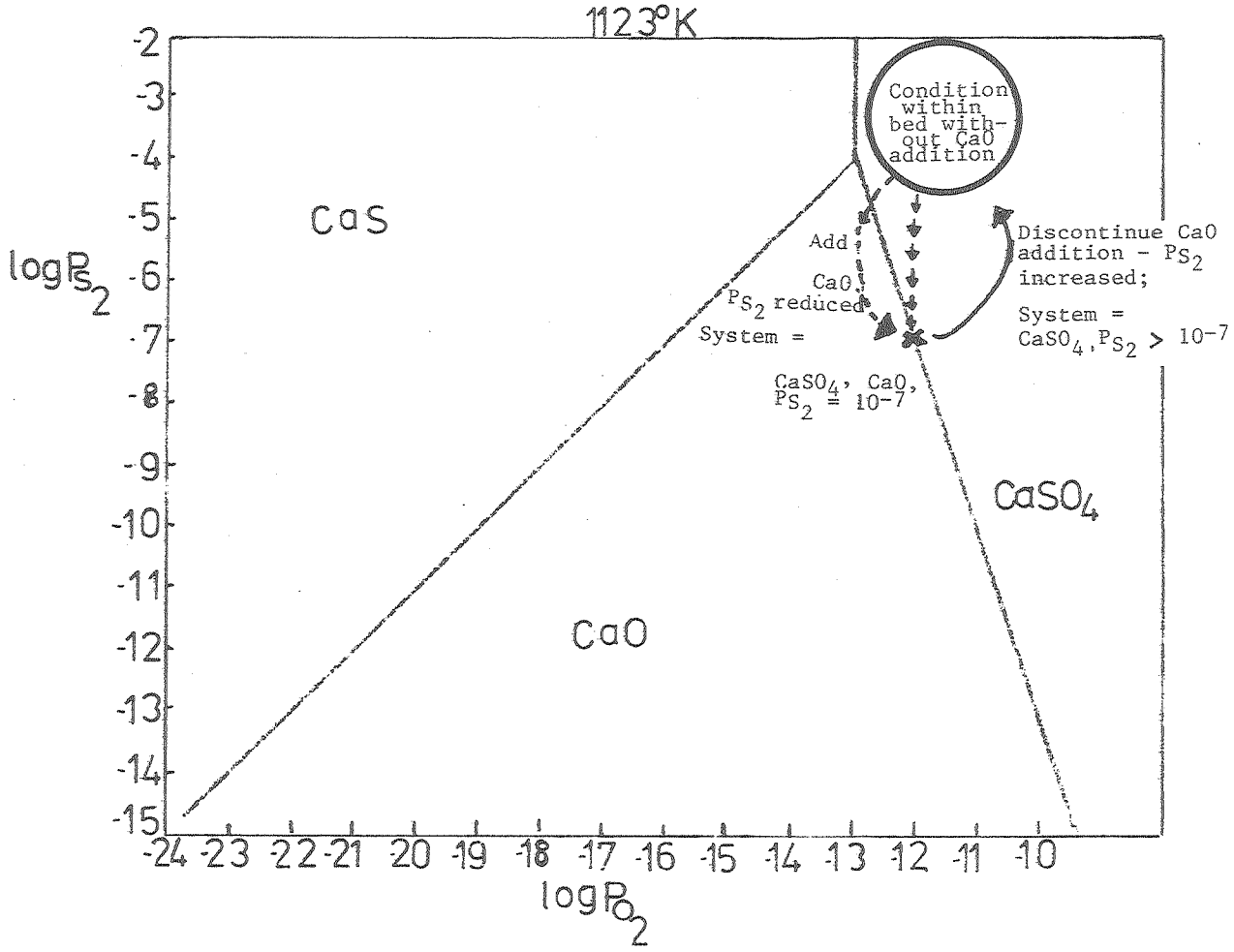

Diagramatic representation of the condition within the fluidised-bed combustor with insufficient CaO at 850°C.

XBL 7911-12795

FIGURE 8

XBB 790-15066

25 μm

Cross-section of the scale formed on In 800 after oxidising in $CaSO_4$/C mixture at 950°C for 12 hours in static air.

FIGURE 9

Scanning electron image, x-ray maps, and Edax analysis results of the cross-section of the scale formed on In 800 after oxidising in $CaSO_4$/C mixture at 950°C for 12 hours in static air.

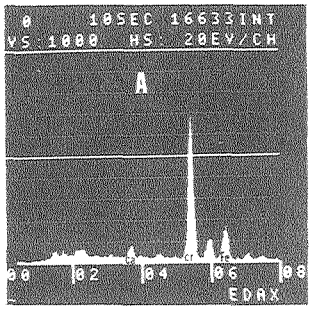

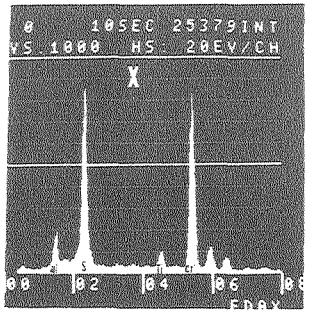

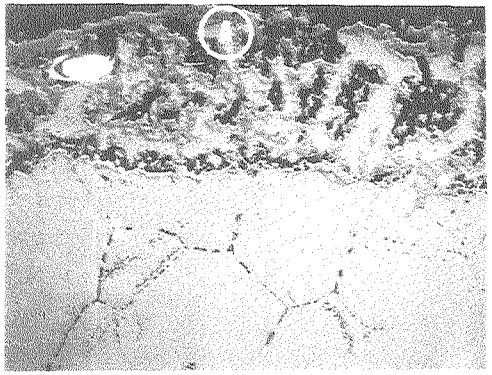

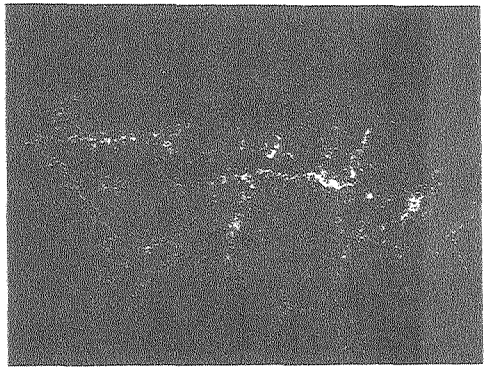

S

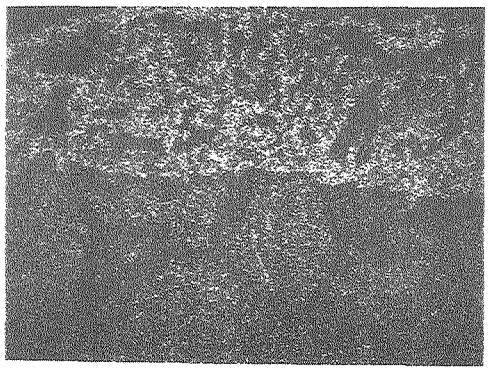

Cr

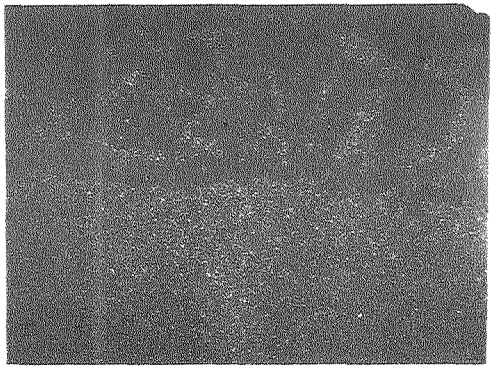

Ni

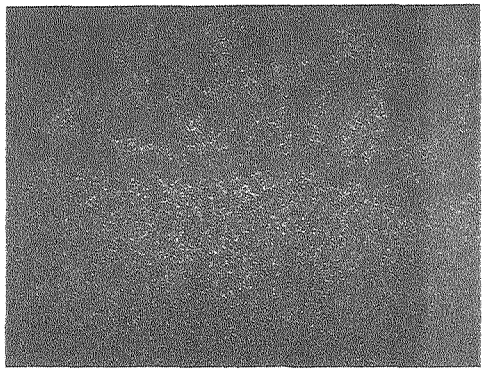

Fe

XBB 790-15069

FIGURE 10

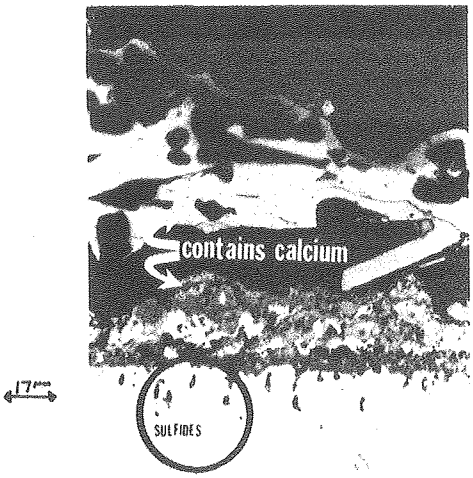

Cross-section of the scale formed on Fe-20C after oxidising in $CaSO_4$/C mixture at 950°C for 12 hours in static air.

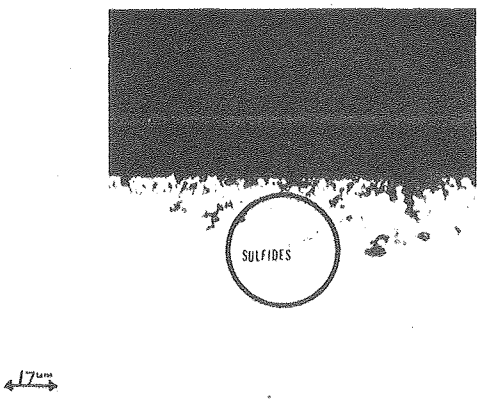

Cross-section of the scale formed on St.St.310 after oxidising in $CaSO_4$/C mixture at 950°C for 12 hours in static air.

XBB 790-15061

FIGURE 11

Cross-section of the scale formed on In 800 after oxidising in $CaSO_4/C$ mixture at 950°C for 50 hours in static air.

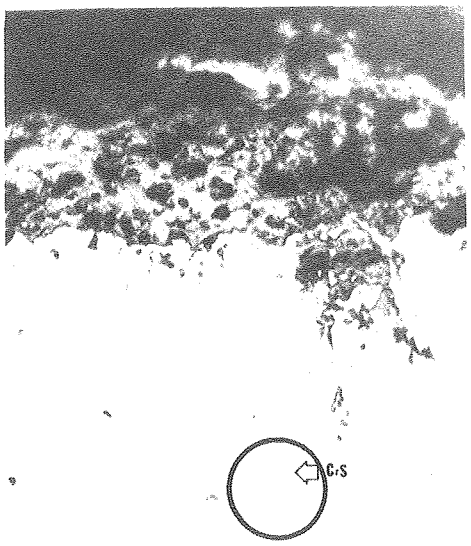

Cross-section of the scale formed on Fe-20Cr after oxidising in $CaSO_4/C$ mixture at 950°C for 50 hours in static air.

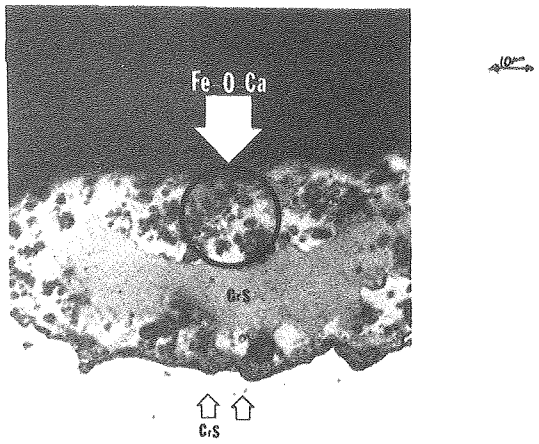

Cross-section of the scale formed on St.St. after oxidising in $CaSO_4/C$ mixture at 950°C for 50 hours in static air.

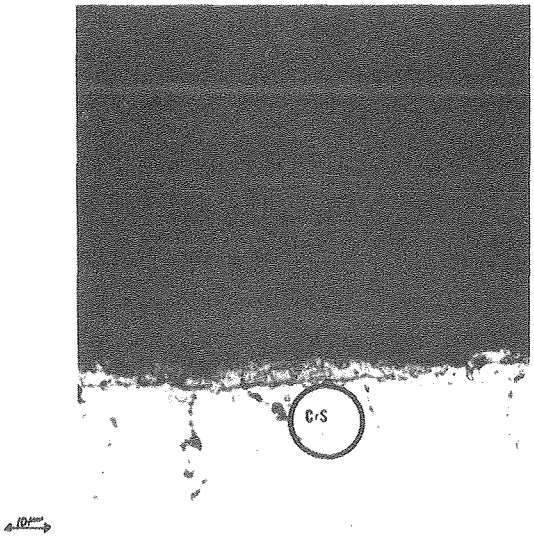

XBB 790-15068

FIGURE 12

SEM and corresponding X-ray maps of the region of the cross-section of the scale on Fe-20Cr with internal sulfide attack after oxidation in CASO4/C at 850°C in static air for 100 hours.

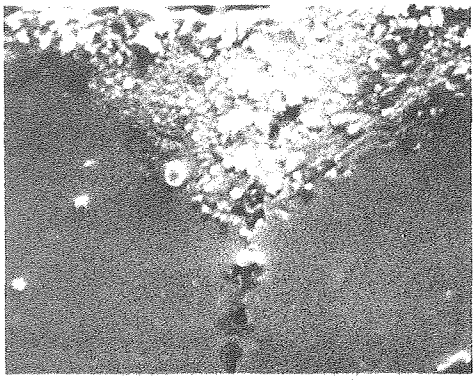

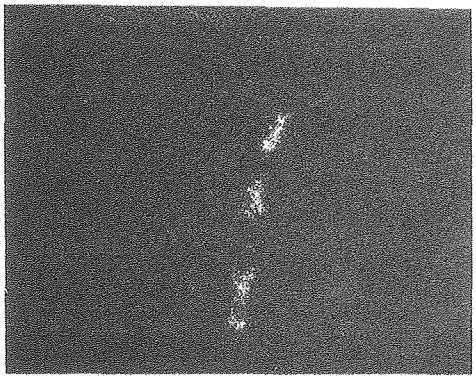

S

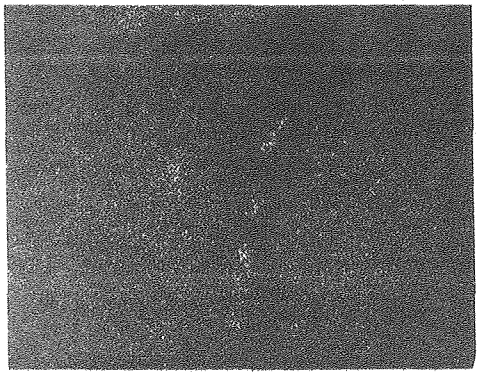

Cr

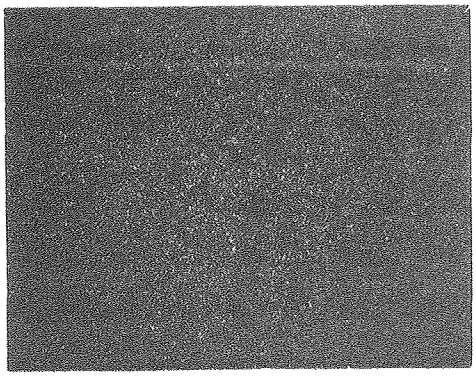

Fe

XBB 790-15064

FIGURE 13

Cross-sections of the scale formed on In 800, Fe-20Cr and Stainless Steel 310 after oxidising in $CaSO_4/CaO$ at 850°C and $P_{O_2} = 10^{-19}$ atm. for 100 hrs.

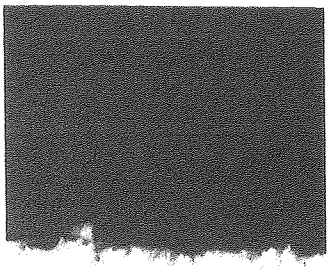

10μm

IN 800

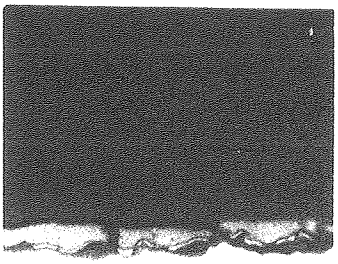

10μm

Fe-20%Cr

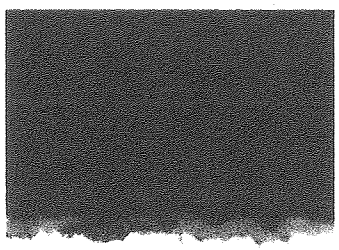

10μm

Stainless Steel

XBB 790-15060

FIGURE 14

Cross-sections of the scale formed on In 800, Fe-20Cr and Stainless Steel 310 after oxidising in CaS/CaO at 850°C and P_{O_2} = 10^{-19} atm. for 100 hrs.

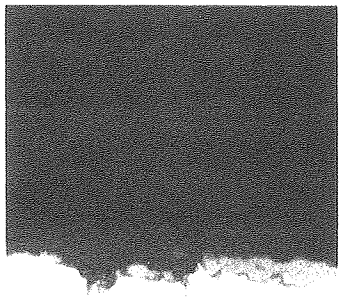

10 μm

IN 800

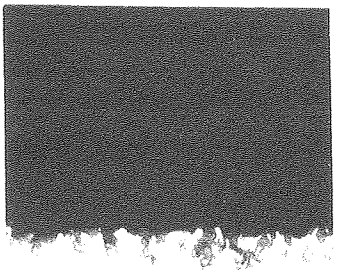

10 μm

Fe-20%Cr

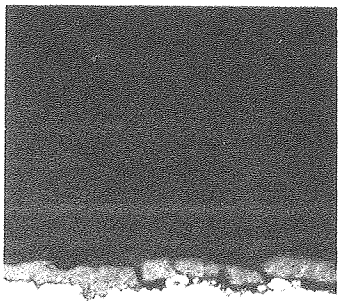

10 μm

Stainless Steel

XBB 790-15059

FIGURE 15

Cross-sections of the scale formed on In 800, Fe-20Cr and Stainless Steel 310 after oxidising in $CaSO_4/CaO$ at 850°C and P_{O_2} = 10-11.5 atm. for 100 hrs.

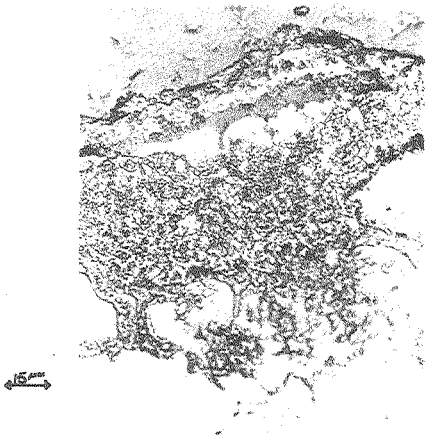

Edge attack

IN 800

Side attack

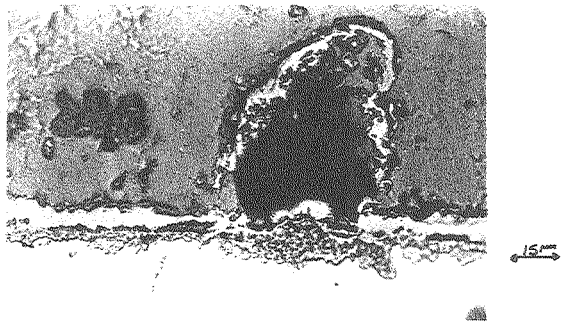

IN 800

Fe-20%Cr

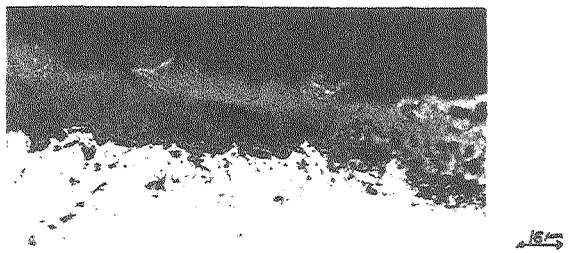

Stainless Steel 310

XBB 790-15067

FIGURE 16
Scanning electron image and x-ray maps of the scale formed on Fe-20Cr after oxidising in $CaSO_4/CaO$ at 850°C and P_{O_2} = 10-11.5 atm. for 100 hrs.

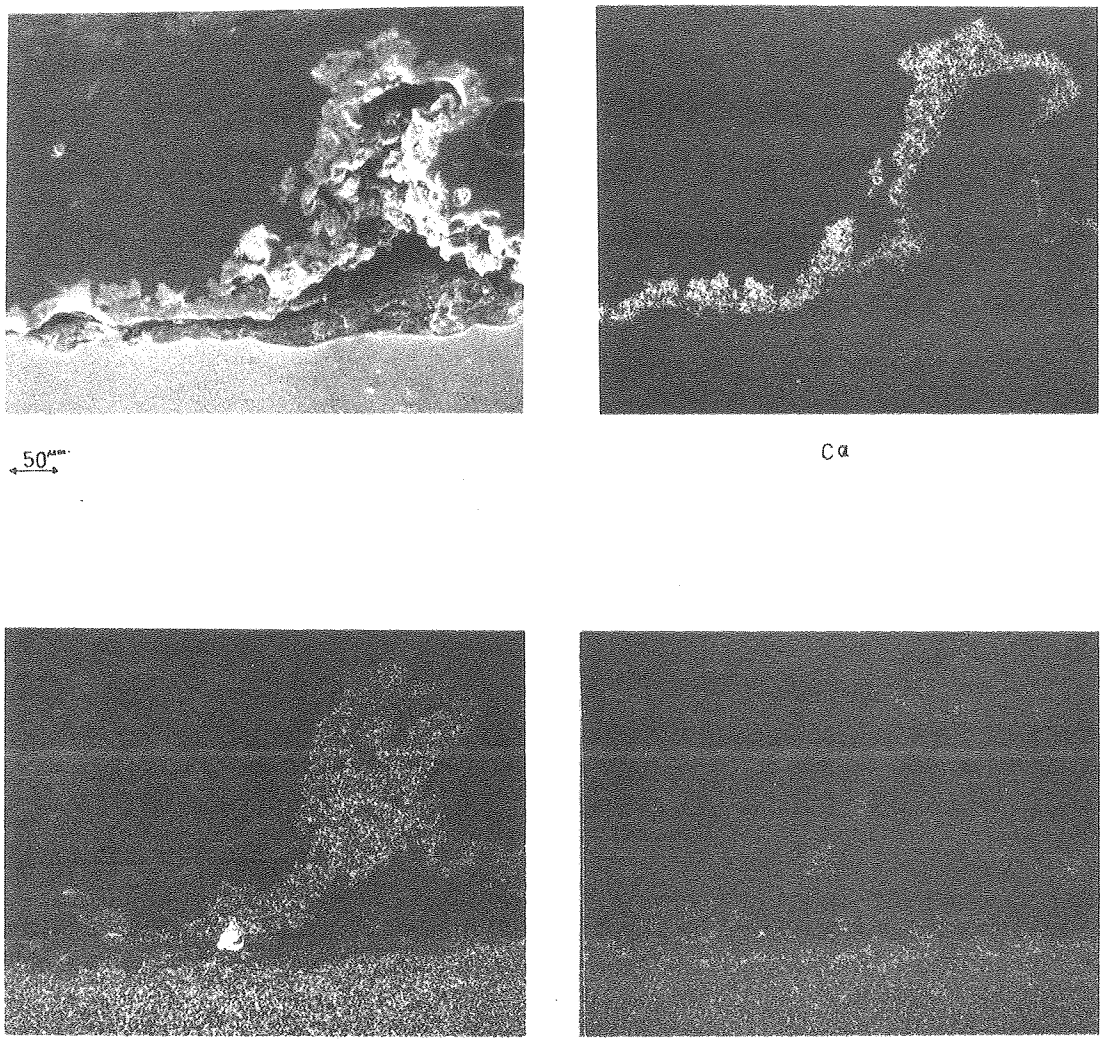

XBB 790-15062

FIGURE 17

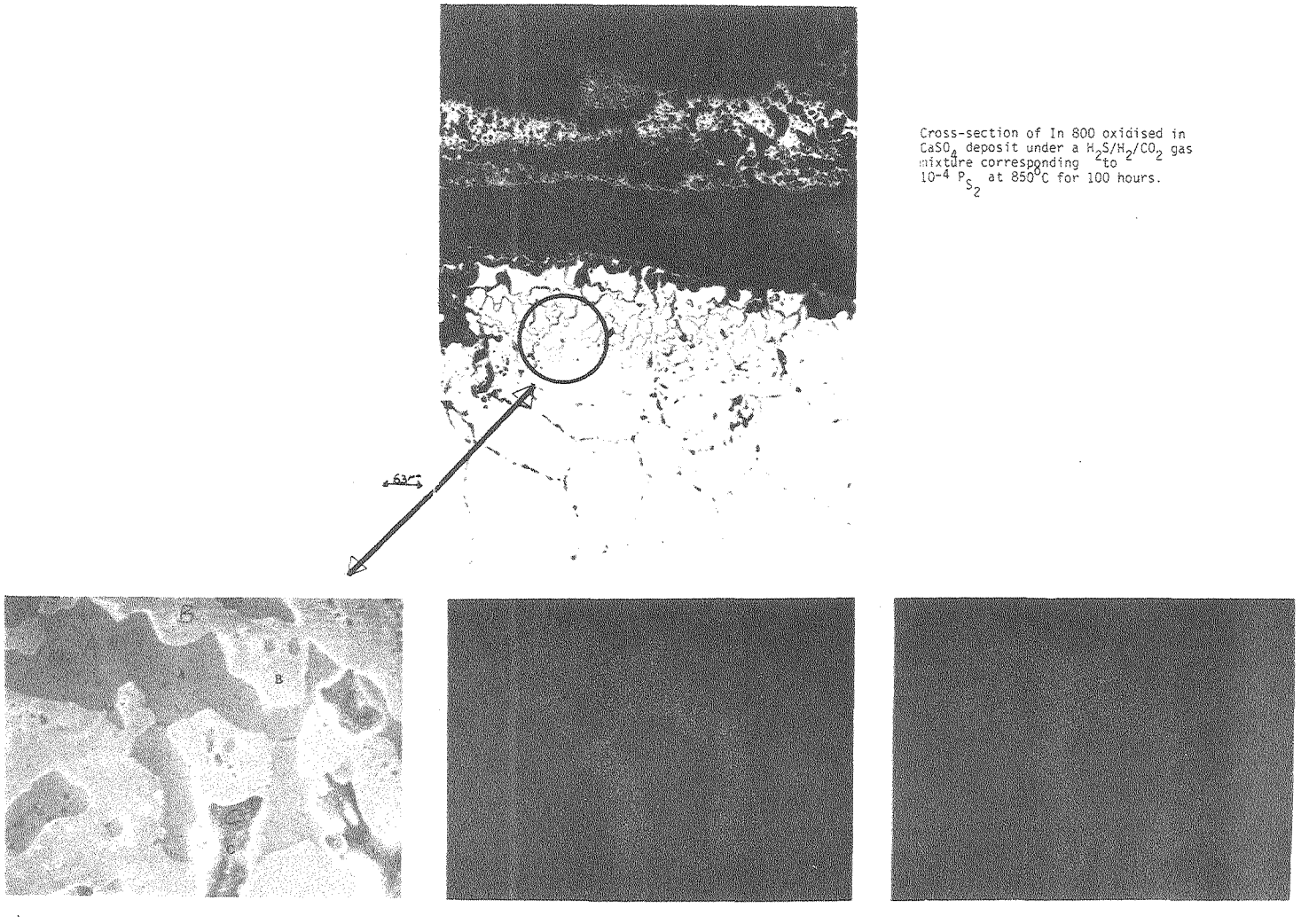

Cross-section of In 800 oxidised in $CaSO_4$ deposit under a $H_2S/H_2/CO_2$ gas mixture corresponding to 10^{-4} P_{S_2} at 850°C for 100 hours.

XBB 790-15059

FIGURE 18

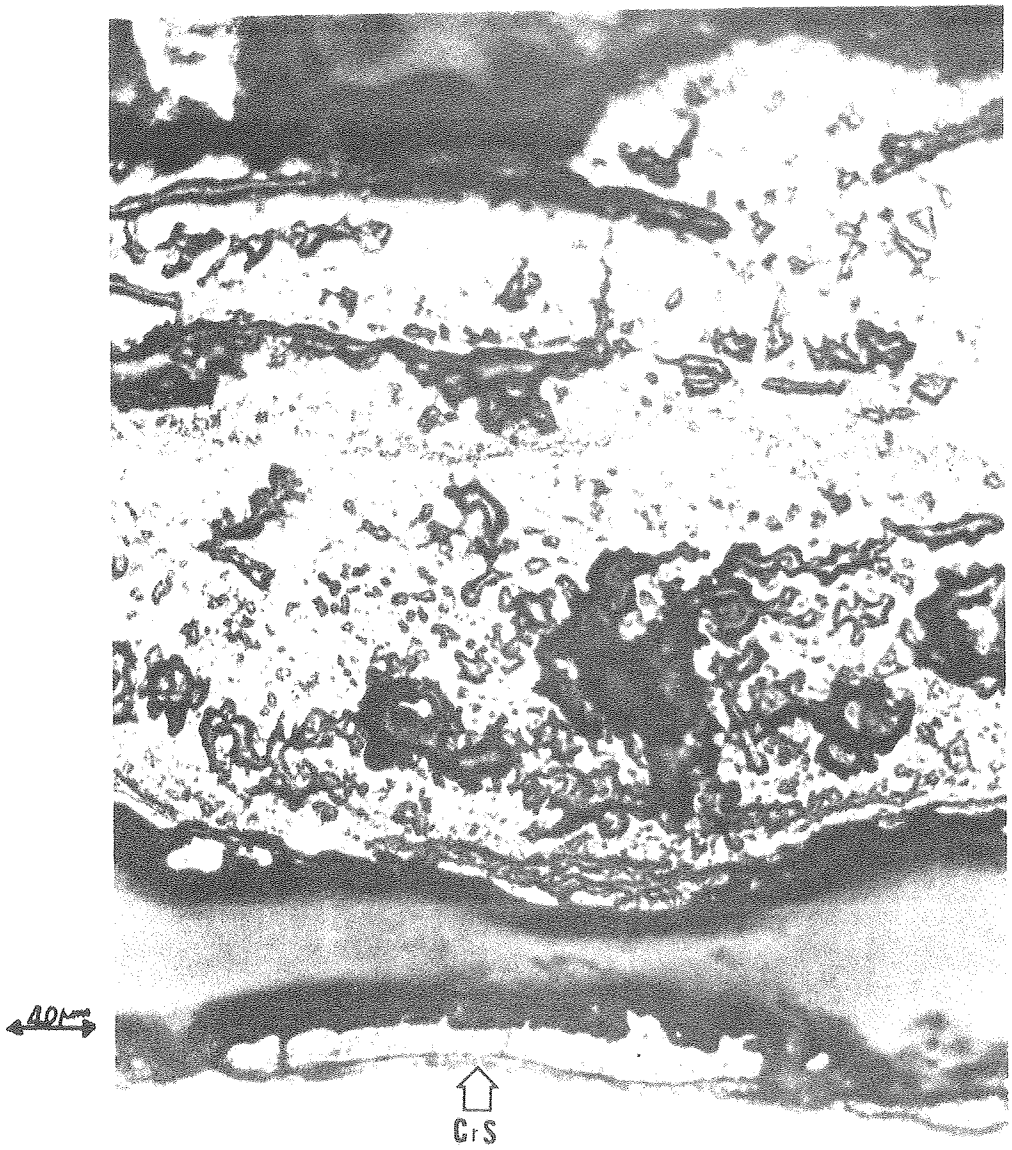

XBB 790-15065

Cross-sections of Fe-20Cr oxidised in $CaSO_4$ deposit under a $H_2S/H_2/CO_2$ gas mixture corresponding to 10^{-4} P_{S_2} at 850°C for 100 hours.

FIGURE 19

Cross-sections of In 800 and St.St. 310 oxidised in $CaSO_4/NH_3$ vapor at 850°C for 60 hours in static air.

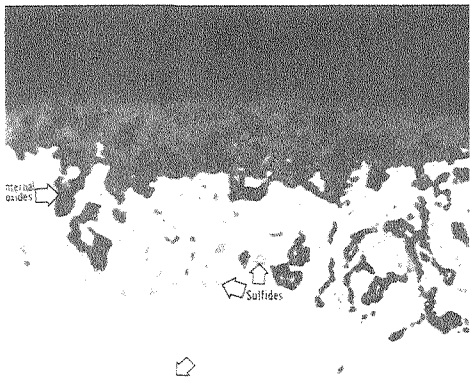

10 µm

IN 800

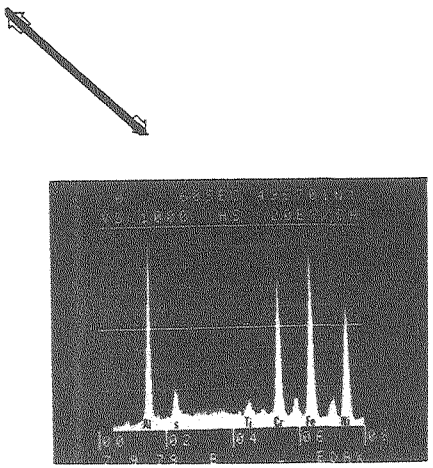

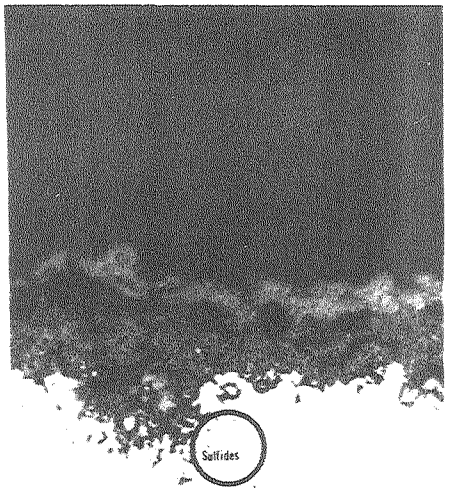

17 µm

Stainless Steel

XBB 790-15057

FIGURE 20

Cross-sections of In 800, Fe-20Cr and St.St.310 after oxidation in $CaSO_4$ at 1100°C for 3 hours in static air.

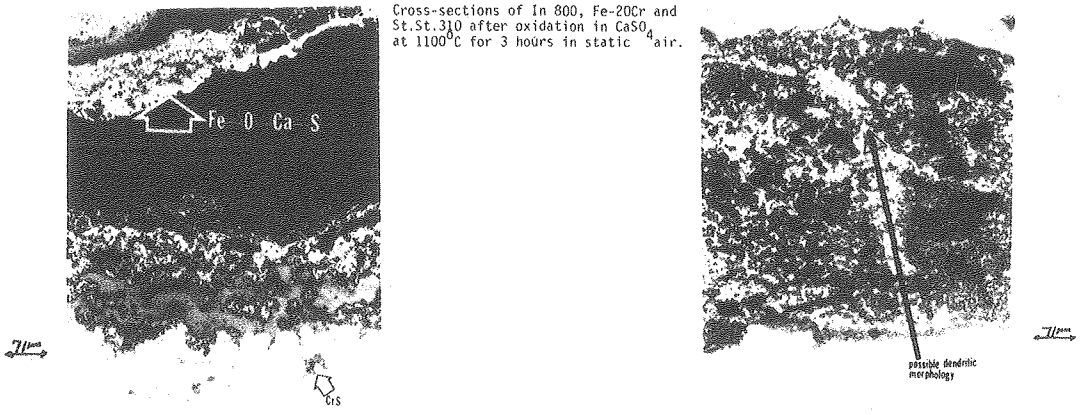

IN 800

Fe-20Cr

Stainless Steel

XBB 790-15056

FIGURE 21

Cross-sections of In 800, Fe-20Cr and St.St.310 after oxidation in $CaSO_4$ at 1050°C for 20 hours in static air.

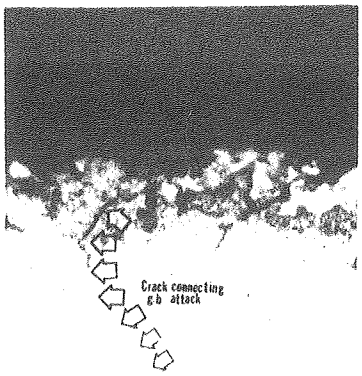

10 μm Stainless Steel

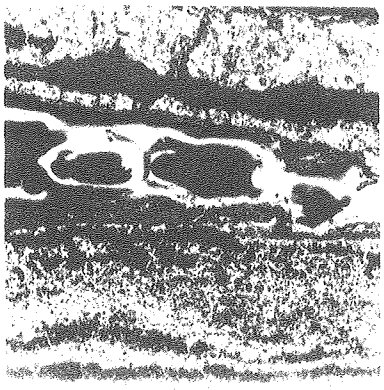

125 μm Fe-20%Cr

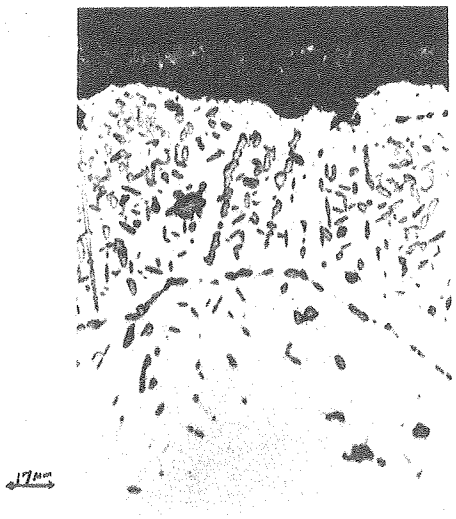

17 μm IN 800

XBB 790-15055

FIGURE 22

Cross-sections of scales formed on pure Nickel, pure Iron and Pure Chromium after oxidation in $CaSO_4/C$ for 11½ hrs. at 850°C in static air.

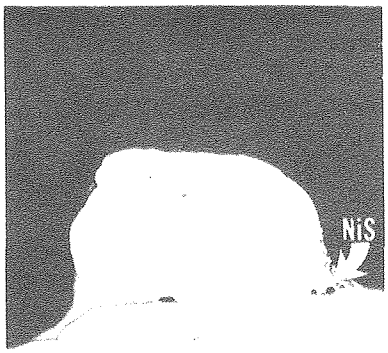

25μm

PURE NICKEL

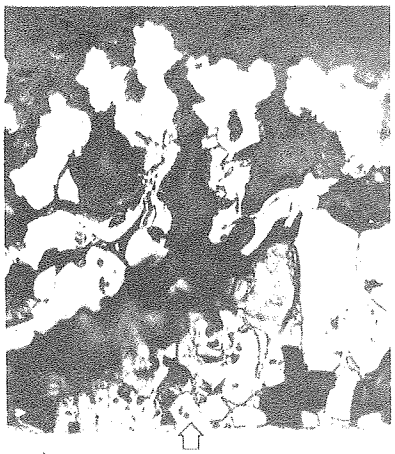

25μm

Pure Iron

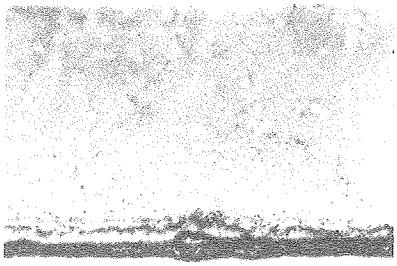

25μm

Pure Chromium

FIGURE 23

Cross-sections of the $CaSO_4$/iron and $CaSO_4$/iron oxide interface during oxidation in a hot stage microscope in the temperature range 19°C to 850°C.

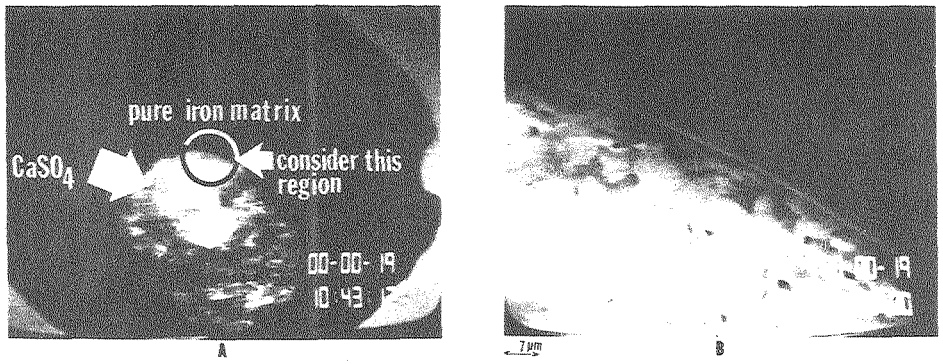

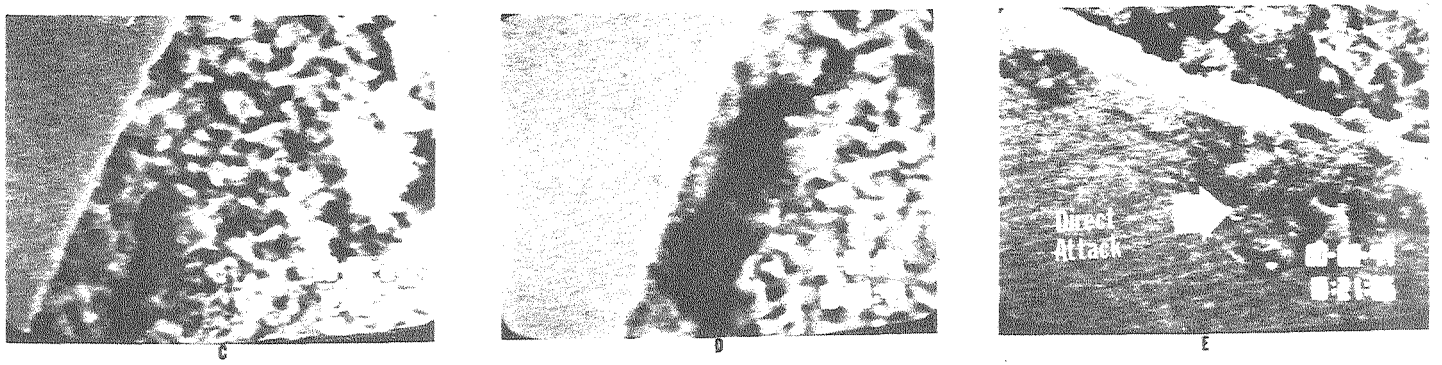

XBB 790-13053

FIGURE 24

Scanning electron image and X-ray maps of $CaSO_4$/iron oxide interface after oxidation in a hot stage microscope at 850°C.

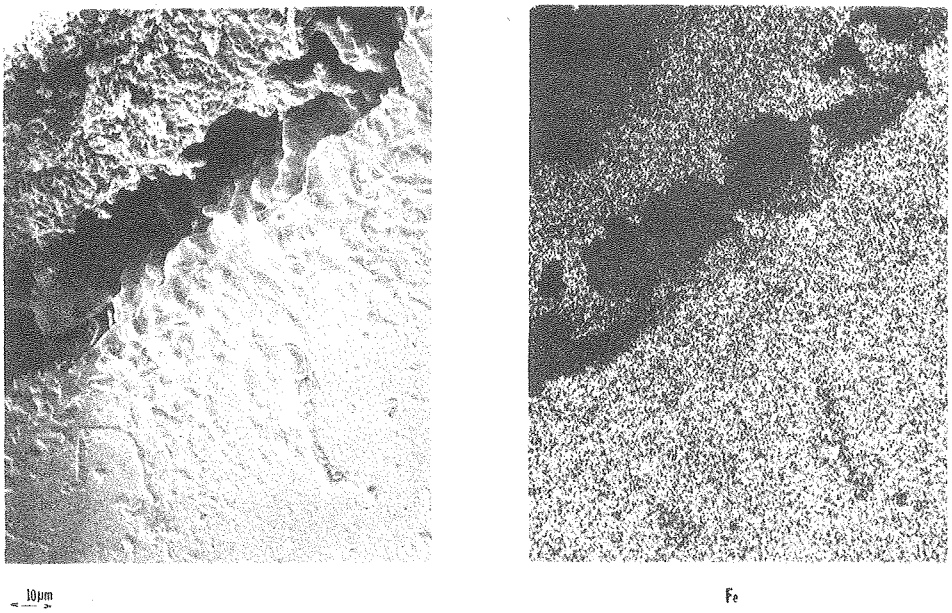

XBB 790-15063

FIGURE 25

SECTIONS showing the response and subsequent melting of the product of $CaSO_4$-Fe interaction within the range 851 - 957°C in a hot stage microscope.

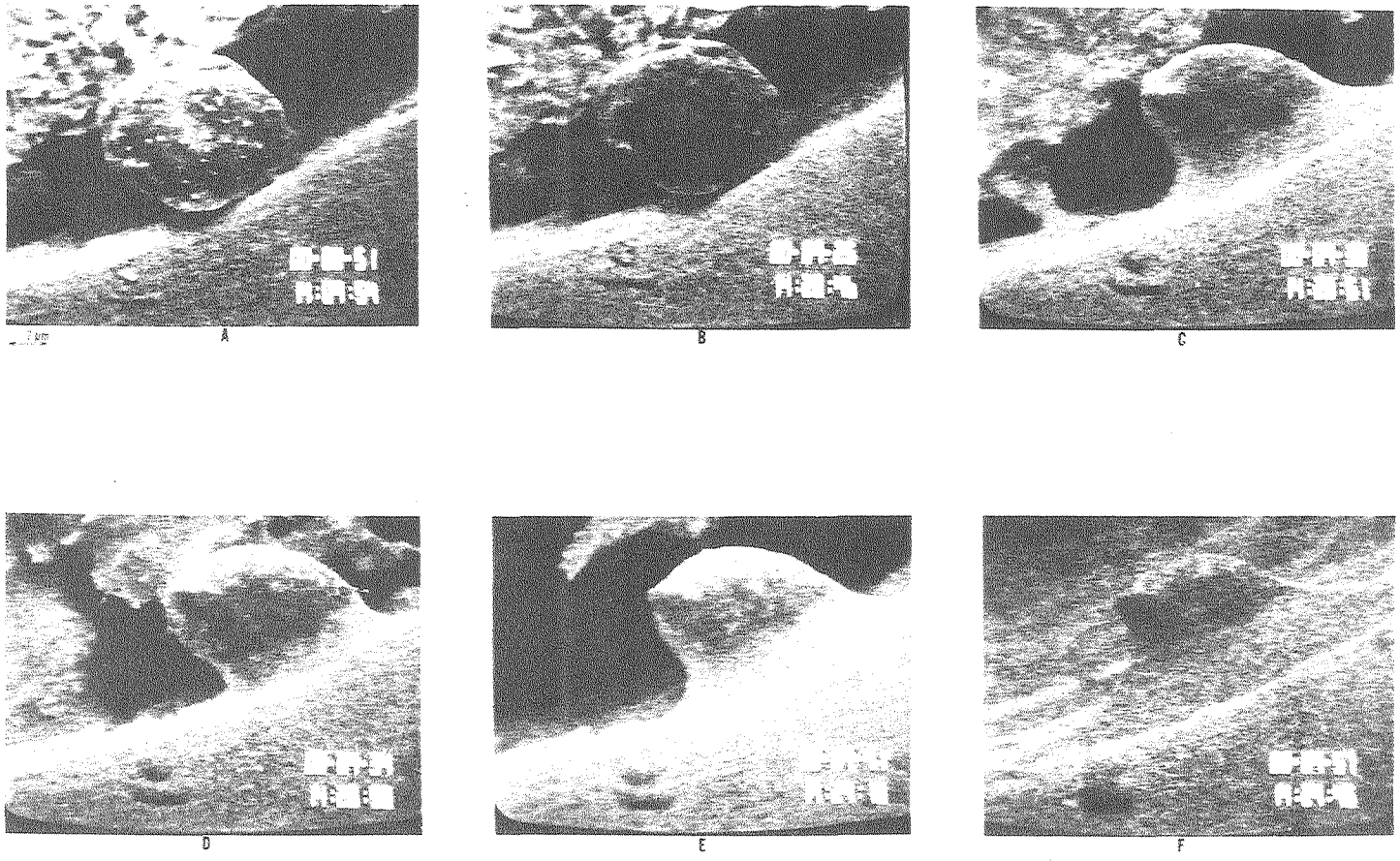

XBB 790-15052

FIGURE 26

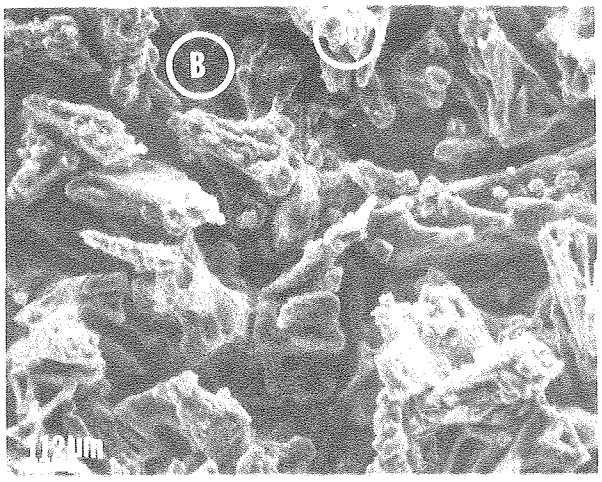

Scanning electron image of pure Iron after oxidation in $CaSO_4$ at 1050°C for 2 hours in static air.

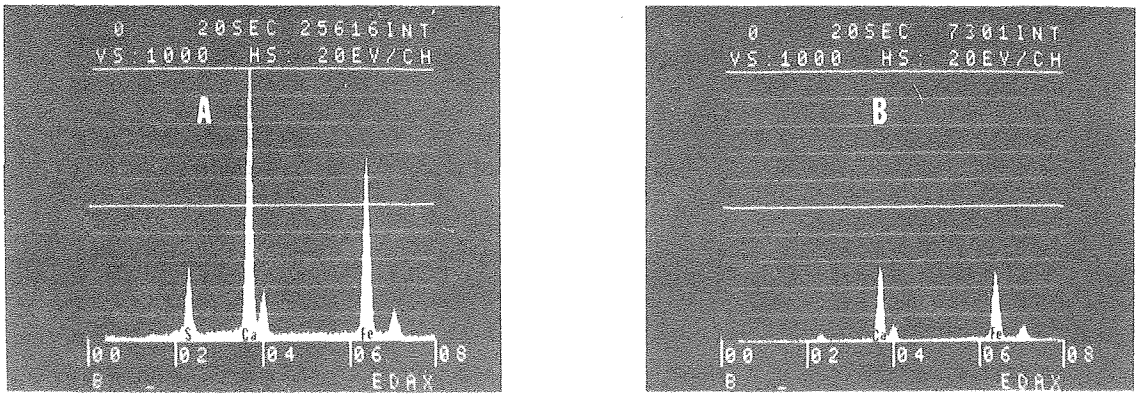

XBB 790-15051

Edax analysis results of regions 'A' and 'B' above.

FIGURE 27

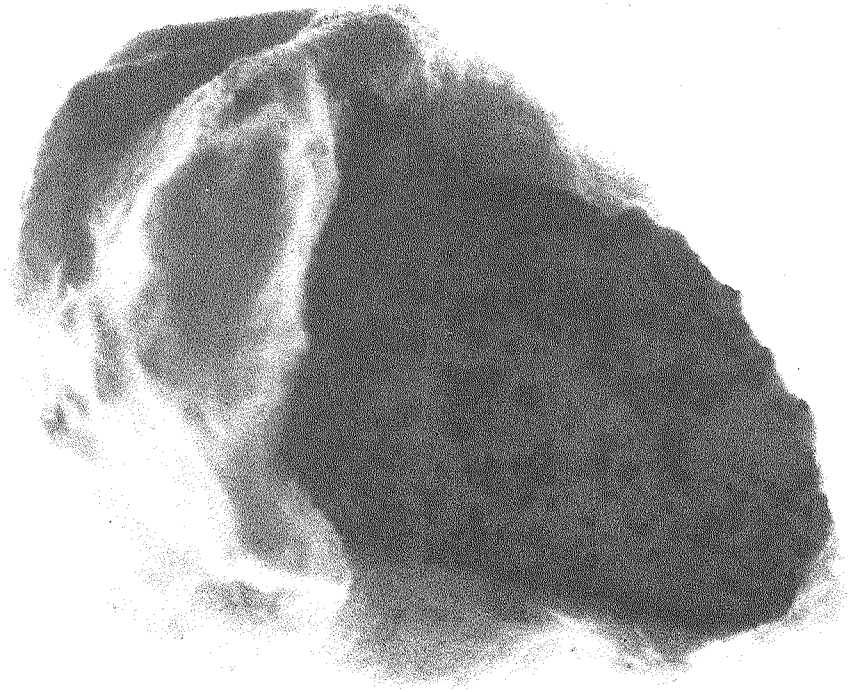

SECTION showing the $CaSO_4$ deposit lying next to the oxide after oxidation at 850°C.

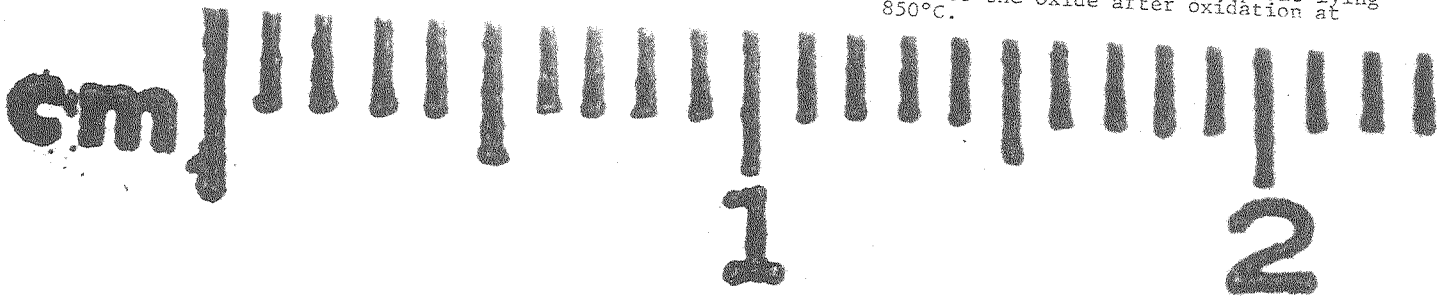

CEE 798-10659

FIGURE 28

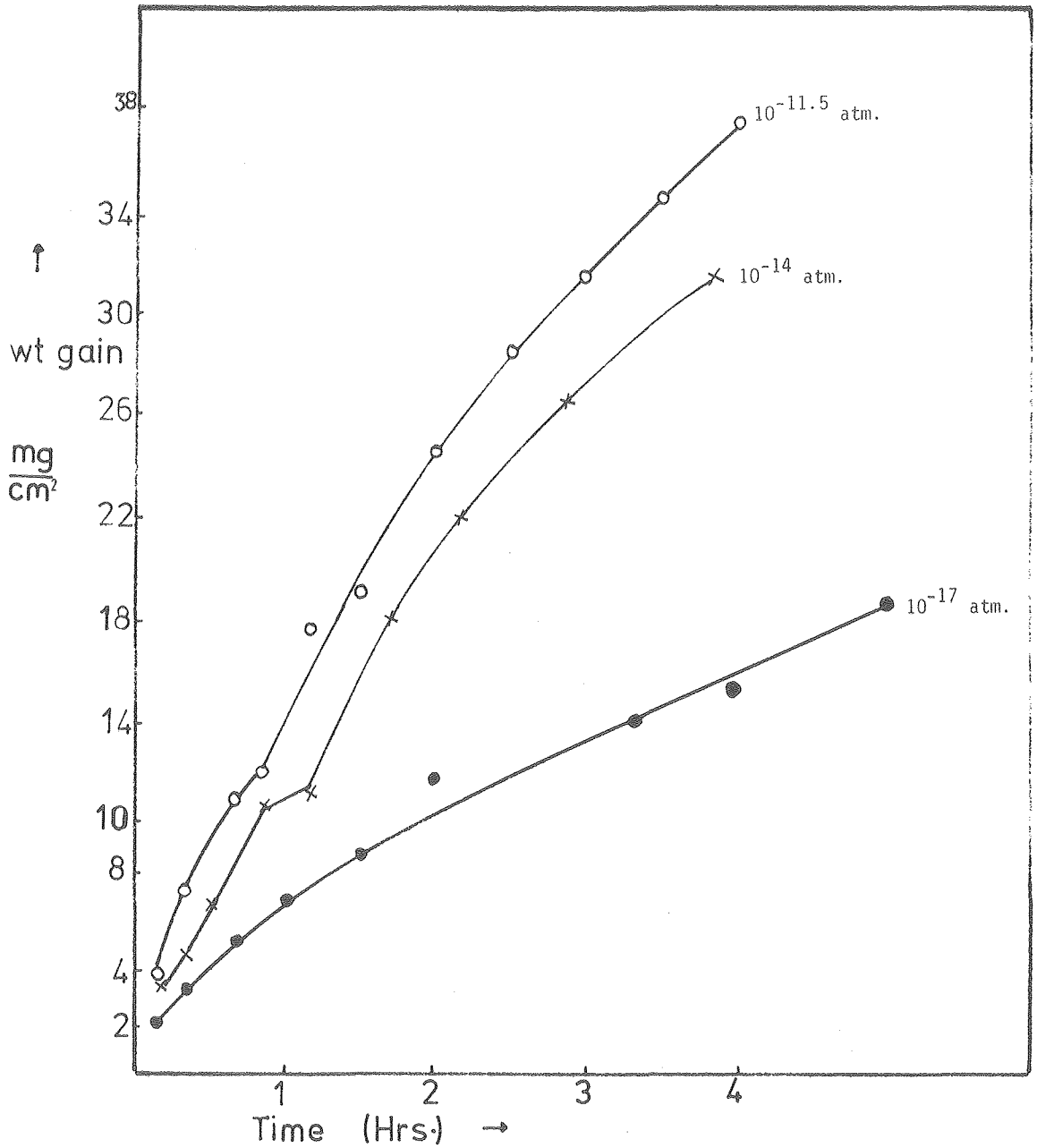

Weight gain versus time for pure iron after oxidising coated with $CaSO_4$ at 850°C in various oxygen activities.

XBL 7911-12899

FIGURE 29

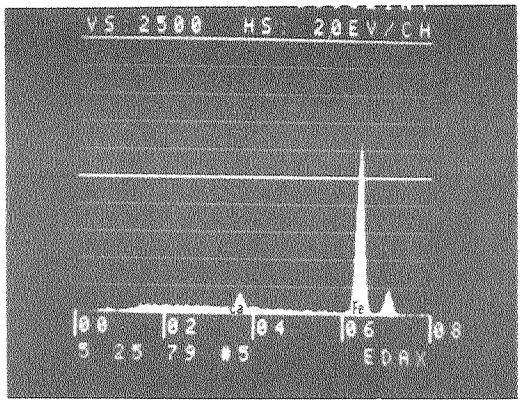

B

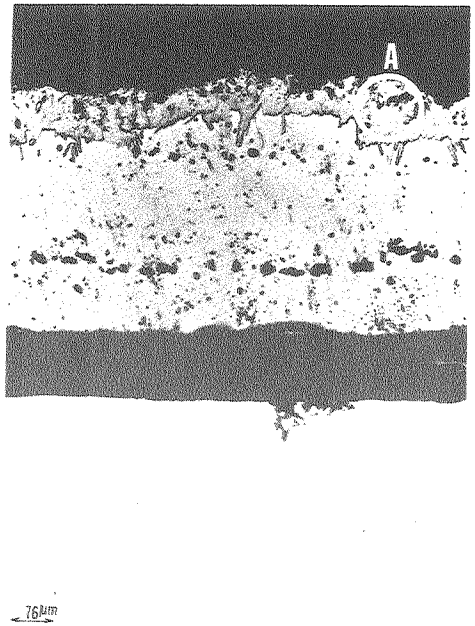

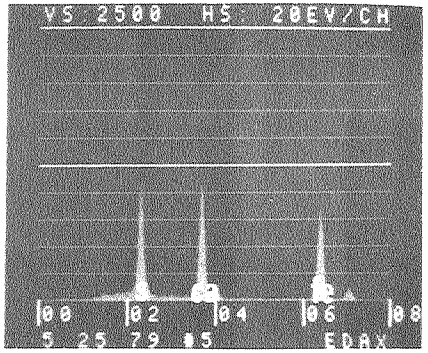

A

Cross-section of the scale formed on pure iron after oxidation in $CaSO_4$ deposit at 850°C for 3 hours and $P_{O_2} = 10^{-19}$ atm.

XBB 790-15050